

Applying a Commercial Atomic Force Microscope for Scanning Near-field Optical Microscopy Techniques and Investigation of Cell-cell Signaling

Gabriela Monserratt, López Ayón

Master of Sciences
Department of Physics
McGill University
Montreal, Quebec
2009-12

Thesis submitted in partial fulfillment of the requirements of the
degree of MSc.

© Gabriela Monserratt López Ayón, 2009.

DEDICATION

To: all those who leave their families and countries to pursue better opportunities in life, to all their families too.

ACKNOWLEDGEMENTS

I acknowledge my mom and my family for all their love, constant support and patience. Thanks for believing in my dreams.

I want to foremost acknowledge my supervisor, Dr. Peter Grütter, for his great humanity, his emotional and intellectual support, constant guidance, inspiration and wise advice. Thank you for motivating my interest in my work and motivate my creativity.

I would specially acknowledge Jeffrey Le Due for his patience and enthusiasm, for all his smart advice and experience. Thanks for helping me to learn, believing in me and making me feel I'm a capable person.

I would like to thank Dr Svetlana Komarova for all her guidance in the Bone Cell project and for encouraging me to try new things. You really kept me excited about my work. I would like to include in this part Osama Maria, with whom I worked closely and from who I learned about cells and life.

In addition, I acknowledge all the people with whom I worked in the lab, especially Dr Helene Bourque for all the interesting discussions and emotional support, Dr Yoichi Miyahara for all the experimental guidance, and all the other students who collaborated in this work.

For financial support, I would like to acknowledge McGill University, the Physics Department, the Center for Materials Physics and my supervisor Dr Grütter for funding my studies.

Thanks to you and all my friends for your time and for making life fun with your friendship.

ABSTRACT

The field of research of this thesis is Condensed Matter Physics applied to Biology. Specifically it describes the development of different Atomic Force Microscopy techniques and tools towards the study of living cells in physiological solution. Particular interest is put into the influence of noise in the determination of ordered liquid layers above a mica surface, as work towards the study of the role of water and ions in biological processes, a "diving bell" array to boost the Q factor to allow stable imaging and force spectroscopy with tips based on Scanning Near Field Optical Microscopy [LeDue, 2008] which are planned to further provide a method of combining both high resolution mechanical and fluorescence studies of bio molecules and cells in solution, and as an application of combined force spectroscopy and fluorescence to biological samples, a study of the mechanical properties and the signaling pathways induced by mechano transduction at the cellular level in bone cells. This investigations have been carried out with the aim to combine Atomic Force Microscopy techniques to achieve force spectroscopy related measurements of cells in specifically fluorescently targeted structures in the cellular membrane with local illumination and Scanning Near field Optical Microscopy techniques to minimize the effect of the light dependent breakdown of the chromophores, which generate reactive oxygen species contributing to bleaching and damage in the cell tissues [Pervaiz, 2006].



ABRÉGÉ

CONTENTS

Title Page	i
Dedication	ii
Acknowledgments	iii
Abstract	iv
Abérgé	v
Table of contents	vi
List of figures	vii
List of tables	viii
Introduction and Background	1
Chapter 1. Experimental Methods	5
1.1 Molecular Force Probe 3D BIO Overview	5
1.1.1 The AFM Head.	7
1.1.2 AFM and Optical Microscopy integration	9
1.2 Convenient Optical Configurations for the Inverted Optical Microscope.	13
1.2.1 Phase Contrast and Epi-fluorescence.	14
1.2.2 Total Internal Reflection Fluorescence Microscopy. . .	18
1.3 Environmental Control.	26
1.4 Atomic Force Microscopy.	29
1.4.1 Force Spectroscopy	30
1.4.2 Imaging modes in AFM	35

Chapter 2. Noise in combined optical microscopy and NC-AFM: towards in-vivo hydration measurements 44

2.1 Noise characterization 44



2.2 Noise modeling 44

2.3 Hydration 44

2.3.1 Hydration measurements.44

2.5 Conclusions. 44

Chapter 3. High Q Optical Fiber tips for NCAFM in liquids 45

3.1 Bent fiber probe fabrication 45

3.2 Diving Bell for Liquid Operation 45

3.3 NC-AFM set-up 45

3.4 High Q in liquid using the diving bell. 45

3.5 Imaging and force spectroscopy. 45

3.6 Conclusions 45

4 Application to Biological Samples 46

4.1 Characterization of Mechanotransduction in Bone Cells. ... 47

4.1.1 Bone Cells and Mechanotransduction 48

4.1.2 Force Spectroscopy and Mechanical Stimulation 49

4.1.3 Calcium Signaling in Bone Cells Induced by Mechanical Stimulation of a single Cell 52

4.1.3.1 Calcium Signaling in Bone Cells. 52

4.1.3.2 Force Spectroscopy. 59

4.2 Conclusions	65
General Conclusions and Outlook	67
Appendix A. Laser beam splitter adapted Scanning Near-field Optical Microscopy.....	70
Appendix B. Phase contrast setup.....	71
Appendix C. Absorption and Emission Spectra Fluo-4.....	72
Appendix D. Calcium [Ca²⁺]_i Primary response sequence ...	73
Appendix E. Student's TTEST	74
Bibliography.....	75

LIST OF FIGURES

Introduction

Figure. 1 Scanning Probe Microscopy Principle

Chapter 1

Figure. 1.1 MFP-3D BIO apparatus.

Figure. 1.2 MFP-3D Head and Scanner.

Figure. 1.3 Cascade Camera Quantum Efficiency Graph. In

Figure. 1.4 Photomultiplier Tube Picture

Figure. 1.5 PMT H5920-01 Spectral Counting Characteristic.

Figure. 1.5 SNOM image of Poly-L-lysine Stripes.

Figure. 1.6 Different optical microscopy illumination techniques.

Figure. 1.7 Phase Contrast mechanism.

Figure. 1.8: Objective Lens Illumination.

Figure. 1.9. TIRF laser optics on the back of IX71 microscope.

Figure. 1.10 Modified Semrock FITC 3540-B Filter cube. This

Figure. 1.11 Transition from Epi-fluorescence to TIRF, fluorescent microspheres solution.

Figure. 1.12 Epi-fluorescence beam profile.

Figure. 1.13 TIRF beam profile.

Figure. 1.14 Open Fluid cell configuration. This

Figure. 1.15 Closed Fluid cell sketch.

Figure. 1.16 Force-Distance curves.

Figure. 1.17 Force volume height.

Figure. 1.18 Au Triangles sample in Contact mode.

Figure. 1.19 Tapping Mode Force-Distance curve.

Figure. 1.20 Au Triangles sample in Tapping mode.

Figure. 1.21 Glass surface in NC mode.

Chapter 2

Chapter 3

Chapter 4

Figure. 4.1 Bone Cells Function in Bone Turnover

Figure. 4.2 Cultured Bone Cells.

Figure. 4.3 NCLAuD cantilever tip etched through FIB

Figure 4.4 Bone Cell response to mechanical stimulation.

Figure 4.5 Frequency of Primary responses.

Figure 4.6 Frequency of Secondary responses. This

Figure 4.7 Primary and Secondary responses.

Figure 4.8 $[Ca^{2+}]_i$ Amount per Unit Area in Primary responses.

Figure. 4.9 Approach F-D curve on a cell showing membrane rupture.

Figure. 4.10 Elastic Modulus in different Bone Cells.

Figure. 4.11 Membrane Deformation with speed

Figure. 4.12 Size of osteoblasts and osteoclasts in primary cells.

LIST OF TABLES

Chapter 1

Table. 1.1: Excitation and Emission Spectra of Fluorochromes commonly used in biology.

Table 1.2. AFM Modes Comparison.

Chapter 2

Chapter 3


Chapter 4

Table 4.1 FD curve features for different cell types.


Introduction and Background

The interest of science in understanding the dimensions and properties of molecules and atoms the things are made of, has been one of the main engines powering research in nanotechnology and microscopy.

Only decades ago few people would have believed a single atom could be visualized simply by touching it. The revolutionary discovery from Binnig, Gerber and Quate in 1986 established the foundation for such an unbelievable possibility [Bining, 1986], the Atomic Force Microscope. Only four years before the development of this technique, the seed of Scanning Probe Microscopy, Scanning Tunneling Microscopy, was invented by Binnig and Rohrer [Bining, 1982] (for which they were awarded the Nobel Prize in 1986). Ever since then, SPM has lead to a variety of diverse imaging tools, which are used to characterize and influence the physico-chemical properties of surfaces and nanostructures.

~~High resolution is attainable with these instruments is an important feature of SPM techniques,~~ but the ability to provide different, original information makes these techniques useful also at lower magnifications. By changing the scanning probe, the interaction detected can be modified, probes such as light (UV, VIS, IR, fluorescence), current, pressure, etc... have lately lead to recent great impact discoveries, involving the nano-world on a wide range of fields for example: d monolayers, self-assembly structures at interfaces, solid surfaces, thin-film technology, interactions at surfaces of ion beams and laser damage, nanoetching and nanolithography, nanotechnology (in diverse applications: nanomachining), atomic switches, mineral surface

morphology, microfabrication techniques, catalyses, single-molecule studies, synthetic polymers, biopolymers (peptides, proteins, DNA, cells, virus), vaccines and biosensors[Birdi, 2003].

The basic principle of all these SPM techniques relies on the vinyl record player principle (a metallic  needle working as a probe used for converting mechanical vibrations to musical sound). SPM techniques essentially rely on a tip moved over a surface. In the case of AFM the tip works as a sensor (probe) with molecular sensitivity (in the order of nanometers) in the longitudinal and height directions.

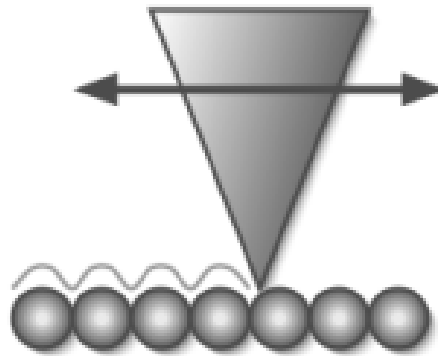


Figure. 1 Scanning Probe Microscopy Principle. This figures illustrate in (a) a vinyl record player needle converting the surface features into sound (image taken from Wingnut Designs), and (b) Schematic of AFM tip scanning across a surface sensing the variations in height over the atoms. Note SPM the probe scanned determines the magnitude measured.

According to the probe, the sensor movement is controlled by a highly sensitive feedback system, which coupled to a variety of signals is capable of providing surface atomic detail. ~~This fact provides attainable work in a new dimension in the "nano meter (10^{-9} m) scale" to the surface research area.~~ Due to these developments, the last decades have experienced a whole new aspect of science, the so called "nanotechnology".

Another highlighting episode came soon after the AFM to contribute to the outreach and expansion of SPM techniques. The Hansma group demonstrated the possibility to image proteins in their aqueous environment [Marti, 1987], [Drake, 1989], opening with this the door to new exploring ideas for biology. This progress was so stimulating, that soon after, the first experiments in biological membranes were done to

investigate the gap junction (connections between cells, which allow molecules and ions to pass freely between cells) [Hoh, 1991].

~~It is to mention that for the first time in history AFM in liquid environments enabled molecular analysis on cells under liquid, before it, the electron microscope, considered as the most capable microscope by then, was (and remains) capable of working only with solid samples in vacuum systems.~~

Given the boom of techniques developed for SPM, optical microscopy, which resolution was then limited by far field diffraction limit (250-300nm), decided to give a try to this new philosophy creating and pushing the light and the optical microscope to its fundamental limits. Following the idea proposed in 1928 by Singe [Singe, 1962], Near Field Optics could be achieved by illuminating the sample through a microscopic aperture with much smaller dimensions than the optical. This new optical microscopy – SPM combined method, capable of circumventing the light diffraction limit was put together until 1987 by the Pohl group [During, 1987] and with this, Scanning Near field Optical Microscopy was built up.

~~These findings make investigations of live cells attainable by combining fluorescence microscopy and force spectroscopy in aqueous environments of great interest. SPM in liquids, fluorescence methods, and SNOM provide powerful tools to understand cellular mechanisms through protein expression by genetically tagging proteins in cells with fluorophores such as Green Fluorescent Protein [Shaw, 2006]. In this thesis different AFM tools have been developed to for combining SNOM and fluorescence in liquid environments using a commercial AFM.~~

This thesis is organized in four chapters. In the first section, a brief overview of the instrumentation and fundamentals of AFM, optical microscopy and fluorescence microscopy, the techniques which enable studies of the mechanical properties of biological samples in solution. This work was done under instruction of Jeff LeDue, who provided me with the knowledge and specifications to work with these tools and then commissioned me to extend the microscope's capabilities; results 1 and 2, corresponding to sections 2 and 3 are attributed entirely to his work.

The second section deals with dynamic atomic force microscopy using frequency modulation (FM) ~~mode~~. This technique has recently been extended to liquid environments [Fukuma, 2005], and, in addition to atomic scale contrast, it is used to ~~test~~ ordered liquid layers above ~~mika~~. The future aim of this study points towards the study of the role of water and ions in biological processes. ~~Optical microscopy combined with AFM provides an invaluable tool to this aim's fulfillment.~~ Our work is developed in a commercial AFM on top of an inverted optical microscope. Such system is commercially available, but mechanical noise due to vibrations is a major concern, and therefore a study of the noise in the system is included in this section.

The third section presents a tip based on an optical fiber which can operate in liquid using a simple 'diving bell' ~~array~~, which allows only a small portion of the tip to be submerged in the liquid while scanning the surface. The tips used are based on scanning near-field optical microscopy and ~~are planned to further provide a method of~~ combining both high resolution mechanical and fluorescence studies of bio-molecules and cells in solution.

The final section presents an application of AFM force spectroscopy and fluorescence to biological samples in order to study their mechanical properties and the signaling pathways induced by mechano-transduction at the cellular level in bone cells, ~~since~~ bone is known to regulate its morphology to adapt to its mechanical usage [Morel, 2001]. Given that bone cells are known to respond to mechanical stimuli through an increase in their intracellular level of calcium [Hung, 1996], a fluorescent dye was used to detect the changes in the cytosolic free Ca concentration after a mechanical stimuli was provided. This investigation ~~has been~~ carried out in collaboration with Dr. Svetlana V Komarova, at the Faculty of Dentistry, Dentistry Department at McGill University.

The objective of this thesis is to contribute to the ~~combination of~~ Scanning Near-field Optical Microscopy, fluorescence and Atomic Force Microscopy techniques to achieve force spectroscopy related measurements of cells in specifically fluorescently targeted structures in the cellular membrane and utilize the SNOM tip to provide a localized source of light to minimize the effect of the light-dependent breakdown of the chromophores, ~~which~~ generate reactive oxygen species ~~contributing to bleaching and damage in~~ the cell tissues [Pervaiz, 2006].

Chapter 1

Experimental Methods

The instrument used for the experiments described is based on a commercially available Molecular Force Probe -3D System on top of an Inverted Optical Microscope (MFP-3D BIO). Additional optical instrumentation and commercial electronics, designed and specified by Jeff LeDue, were then implemented and commissioned in order to extend the microscope's capabilities.

1.1 Molecular Force Probe-3D BIO Overview

All of the experiments discussed in the next chapters were performed using a commercial AFM from Asylum (the MFM3) mounted on an Olympus Inverted Optical microscope (see g. 1.1). This set-up per se allows simultaneous topographical AFM spectroscopy and high optical resolution imaging and fluorescence. The system is inside a thermal and vibration isolation hood (BCH-45 from TMC) and sits on an active vibration isolation table (TS300 from Table Stable). Since the environmental vibrations play an important role in image quality, it is noteworthy that this microscope resides in the fourth floor of a building, ~~which certainly needs extra care of the noise effects on the data acquired and an adequate isolation system is therefore provided.~~

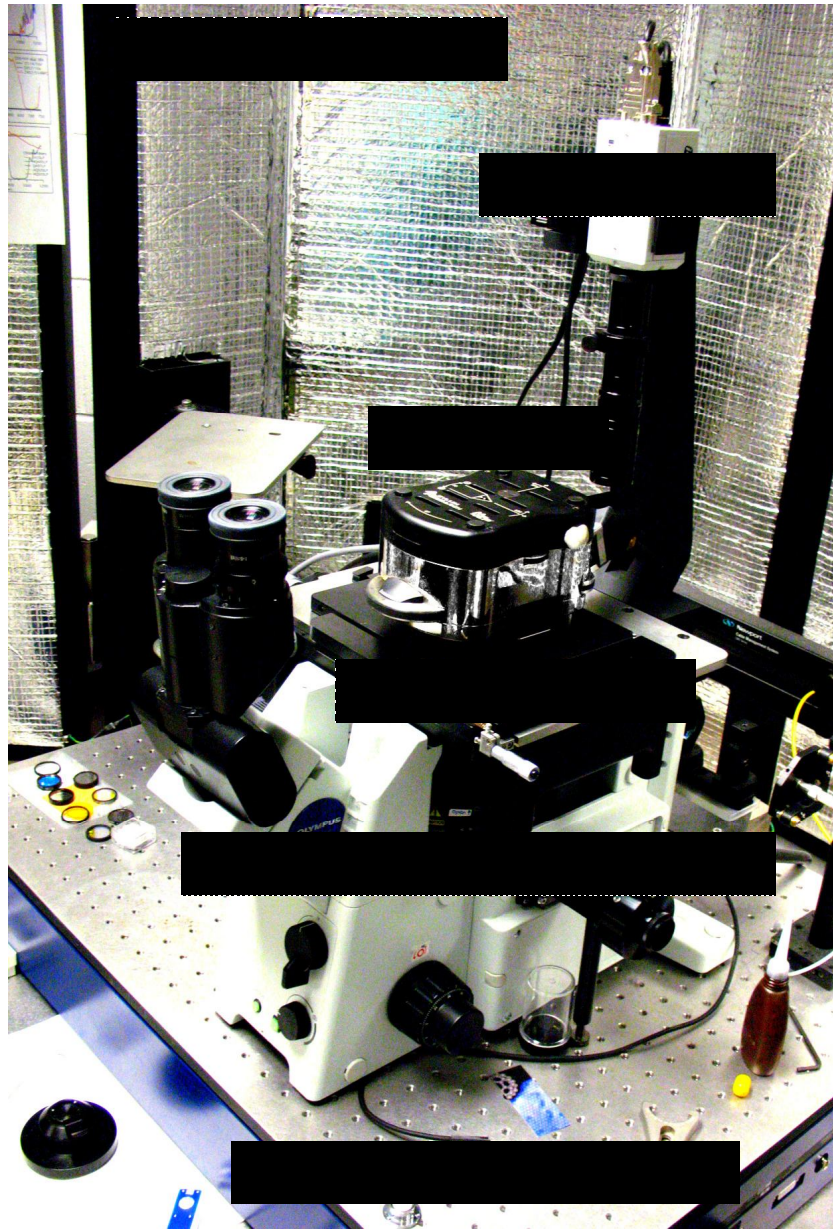


Figure. 1.1 MFP-3D BIO apparatus. This image shows the basic components of the microscope. Labels identifying the commercially available parts of the microscope. The apparatus is mounted on an air table and an acoustic noise and thermal isolation hood, which provide noise isolation. Each of the elements labeled is described in the text.

The sample is mounted on a ~~special~~ holder, which can be magnetically fixed to the scanner. A closed fluid cell for imaging in liquid with heating capabilities can be used. Depending on the nature of the experiment this holder is especially useful for experiments with life biological samples.

In the next sections of this chapter the operation of the individual system components as well as the modifications implemented are described in detail.

1.1.1 The AFM Head

The first key element in our setup is the AFM head. It provides the driving signal to modulate the strength of the interaction between the tip and the sample through the extension and retraction of the **z-piezo**. ~~The ZLVDT (Linear Variable Differential Transformer) acts as a positioning sensing device that measures the distance, it causes the light source-cantilever assembly to move up and down~~ (see g. 1.2).

This microscope is a conventional optical beam deflection AFM, in which the sample is scanned in $x(90\mu\text{m})$ and $y(90\mu\text{m})$, and the head performs the z motion ($16\mu\text{m}$). ~~by scanning the sample, the exact position of each axis is measured and linearized through NPS LVDT (Nano Positioning Sensor-Linear Variable Differential Transformer) sensors, which correct for hysteresis and creep(in the case of the scanner, X-Y direction) and provide accurate force and topography measurements (in the Z direction), allowing to accurately zoom and offset. The latter is particularly important in case an AFM image is panned and overlaid on an optical image. The range over which the LVDT is works within the average deviation of the signal measured in a bandwidth of 0.1 Hz to 1 kHz is 300 pm Z, 600 pm XY, , since at high resolution it leads to excess noise. In the center of the range, i.e. 70 V, the noise may be slightly lower.~~

The light source-detector assembly is composed of a low coherence Infra-Red **light source** (860nm Infra-Red SLD laser) which is aligned to the back of the cantilever, the laser signal is reflected from the back of the cantilever to the segmented **photodiode**, where the intensity of the light is converted into a voltage. The segmented photodiode is made up of a 2X2 matrix in which the difference between the light intensity between the two upper segments and the lower ones gives the **deflection signal**. The location of the laser signal on the back ~~on~~ the cantilever can be monitored using the analog CCD camera positioned on the illumination pillar, which through a 10X objective in the head, detects the image of the cantilever and the laser

being reflected. This camera can also be used to view the top surface of opaque samples.

The **tip holder** in the head allows commercially available **cantilevers** to be used. Both rectangular and triangular tipped cantilevers are compatible with our setup. All cantilevers used had reflective back coatings to improve the signal to noise of AFM measurements. In experiments where the cantilever is completely submerged in liquid only Au coated cantilevers were used since other coatings detach easily under liquid environments.

The **X-Y LVDT** is the scanner, responsible for the sample motion, it works the same way as the ZLVDT, but the stage motion is done through the scanner.

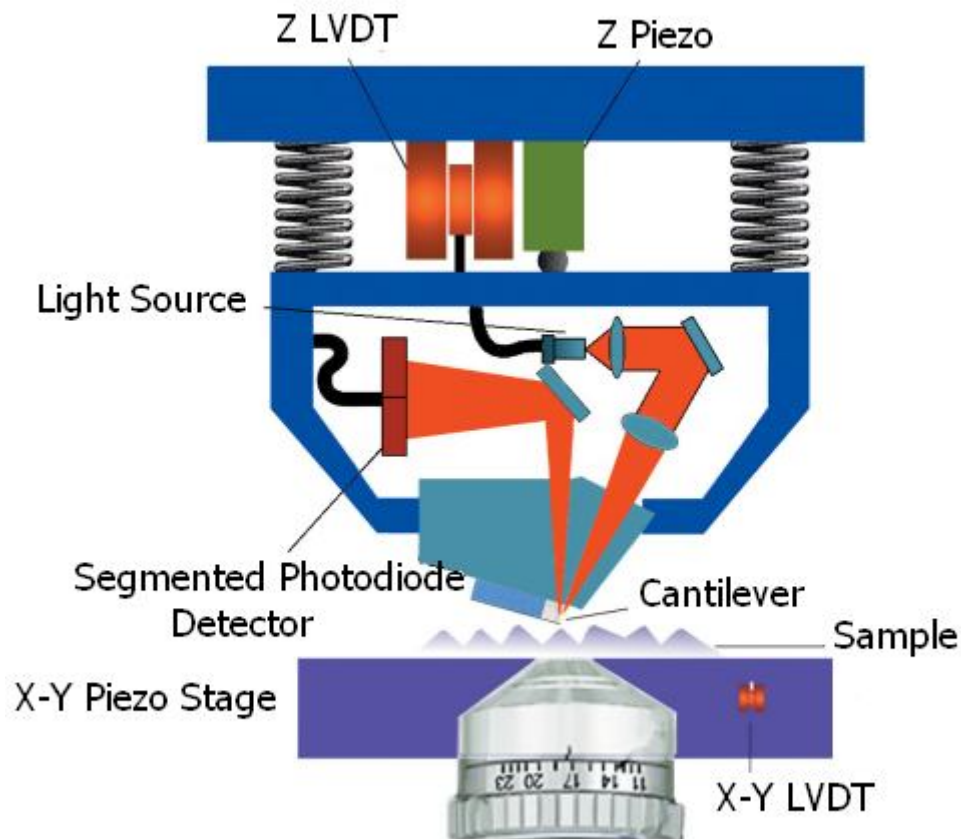


Figure. 1.2 MFP-3D Head and Scanner. In this image a scheme of the interior disposition of the elements in the head is shown. The labels identify the main parts. There is an additional optical part in the head through which the top surface of opaque samples and the alignment of the the 860nm Infra-Red SLD laser are controlled. The

mirror through which the light source is reflected into the photo diode is controlled using one of the knobs on the head, allowing with this to position the beam on the center of the detector. Each of the elements labeled is described in the text.

Image taken from: [Tompkins, 2004]

The optical objective at the bottom of the scanner is used to simultaneously access topographically (through the AFM) and optically transparent samples. In the next section the optical microscopy integration to the AFM system is discussed in further detail.

1.1.2 AFM and Optical Microscopy integration

The optical images in our microscope are acquired through the inverted optical microscope (Olympus IX71), on top of which the AFM and the scanner sit. This microscope can work in simultaneous combination with the AFM.

The illumination pillar, which holds the CCD camera and extends vertically on top of the microscope, and the AFM head serve as the path for the light to illuminate the sample. The light on the sample is then captured by the objective in place. The working objective can be chosen from one of the three (10X, 40X, 60X oil immersion) in the Microscope turret. By adjusting the sample plane, the image acquired is then reflected into the eye pieces for observation. For **image acquisition** or single photon counting measurements, the microscope can optionally be connected to either a cooled CCD camera or other external optical detectors such as a Photo-Multiplier Tube (PMT) through a standard C-mount adapter. In the following paragraphs a brief description of these optical detectors will be provided. For further detail please refer to the manuals cited along the description.

The 512F Cascade Camera is the primary complementary instrument implemented in our setup. It allows us to acquire images using a 512x512 Front-illuminated CCD (Charge-Coupled Device) with 16x16 μm pixels and can be thermo-electrically cooled to -30 °C. This camera uses a unique CCD capable of multiplying the charge (provided by the electrons), generating the pixels. It works using the same principle as the PMT described below [Photometrics, 2004]. Figure 1.3 shows the graph of the Cascade's quantum

efficiency; i.e. the current that a given area will produce when illuminated by a particular wavelength. When the multiplication is sufficiently high, it is possible to see extremely low-light events, note this happens only in a band of wavelengths (see fig. 1.3) as will be furtherly specified.

The capabilities of this camera make it suitable for experiments on Ultra-low light fluorescence, Total Internal Reflection Fluorescence (TIRF), Single Molecule Fluorescence, Spectral imaging and Luminescence. Most of the experiments in this thesis show images and movies acquired with this camera.

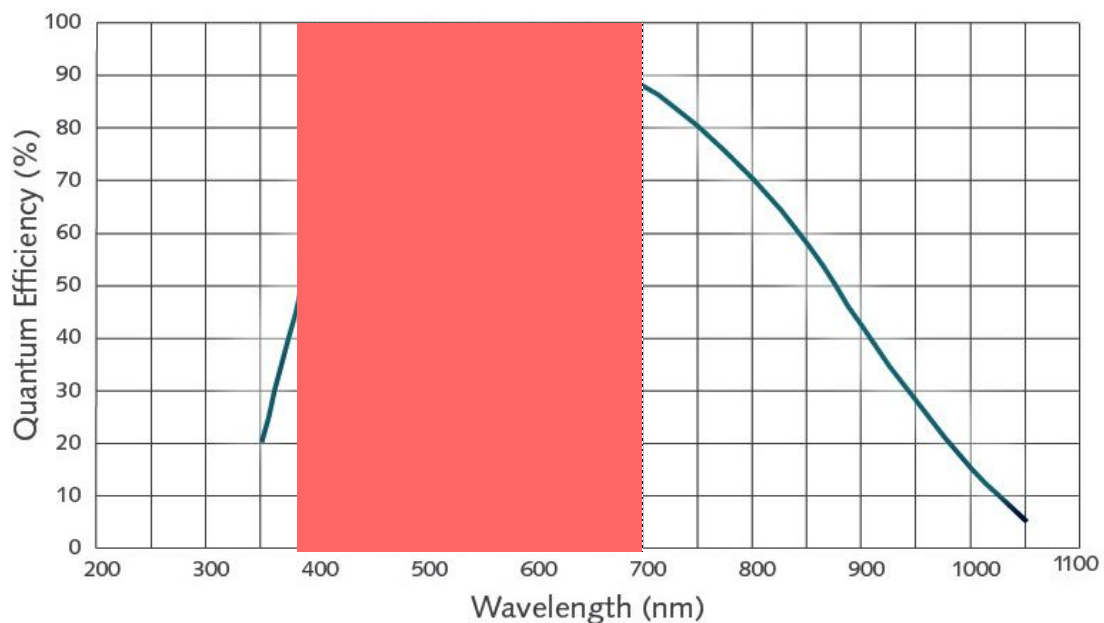


Figure. 1.3 Cascade Camera Quantum Efficiency Graph. In this graph, the percentage of photons hitting the photoreactive surface that will produce an electron-hole pair is plotted against the incident light wavelength. The band represented in the picture corresponds to the visible light spectrum; this region is coincident with the region where the camera is most sensitive, however, it may be possible to attain higher acquisition rates for light above the 450nm (blue).

The PMT H5920-01 (integrated photon counting head module using R5610) from Hamamatsu is a versatile device which provides ultra-fast response and extremely high sensitivity for image acquisition [Hamamatsu, 2008]. In it, the photons coming in the photocathode produce a cascade of electrons which number is multiplied by absorption and re-emission between

dynodes, which amplify the signal (see fig. 1.4). After amplification, the resulting electrons are detected as an output signal in the anode.

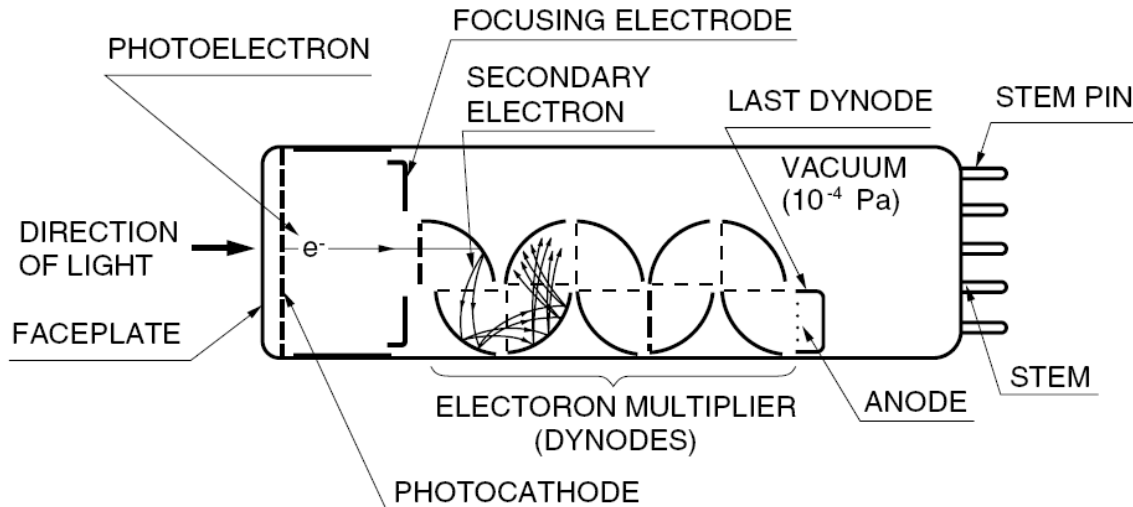


Figure. 1.4 Photomultiplier Tube Picture. In this picture the basic operating characteristics of the PMT are shown. The photomultiplier tube allows photon counting in extremely low light intensity levels such as bioluminescent samples.

The PMT's spectral response range is 300nm - 650nm and has 1/10 prescaler, which improves the count linearity. It is able to detect down to 10 dark counts per second, with a pulse resolution of 5ns and output pulse width of 25ns and maximum count rate of 30Mcps.

This instrument provides exceptionally low noise levels compared to other photosensitive devices, and can be applied to detect a wider range of light (from near ultraviolet to visible red) in the electromagnetic spectrum (compared to the CCD camera, see fig. 1.5) ~~whenever these type of waves are capable of transmitting through the microscope optics.~~ These instruments are widely used for chemiluminescence and bioluminescence measurements.

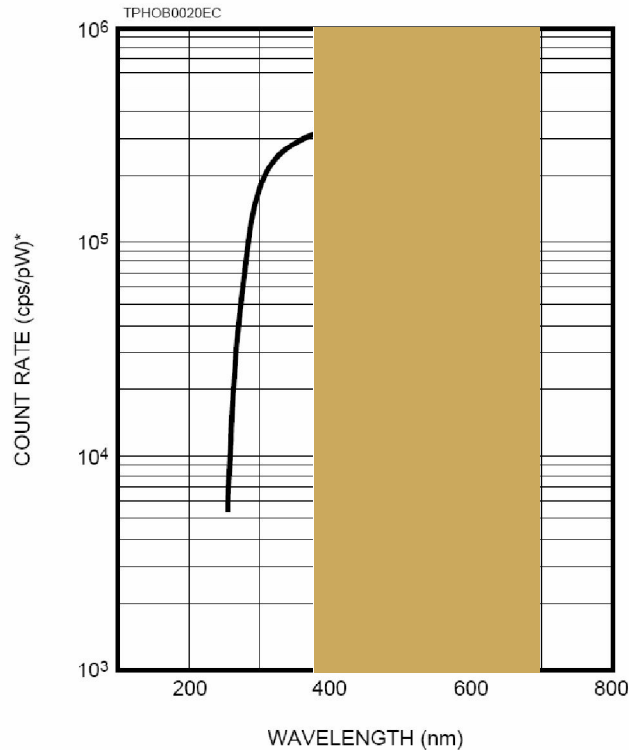


Figure. 1.5 PMT H5920-01 Spectral Counting Characteristic. In this graph, the photon count rate i.e. the number of photons which can be received per second when hitting the photo reactive surface that will produce an electron-hole pair is plotted against the incident light wavelength. Here, again, the band represented in the picture corresponds to the visible light spectrum; suggesting the PMT is more sensitive to lower wavelengths than the camera.

As a final point and contrasting the capabilities of the PMT versus the ones of the CCD camera above described, it is recommended to use the CCD camera when a high resolution image is required for further manipulation, however, the instrument to employ is the PMT when single photon counting resolution is required and a wider range of the electromagnetic spectrum is required. The PMT isn't capable of forming an image of the sample, but it rather counts the number of photons and can be used in combination with Scanning Near-Field Optical Microscopy (SNOM) to form an image of a sample in either collection or emission modes of SNOM. Images in-attained using this technique can reach a resolution below the diffraction limit [Lange, 2001]. In order to facilitate work in the SNOM mode, a laser beam splitter has been adapted (for further details; consult Appendix A). Local illumination and bleaching are easily achievable with this technique as shown in figure 1.4.

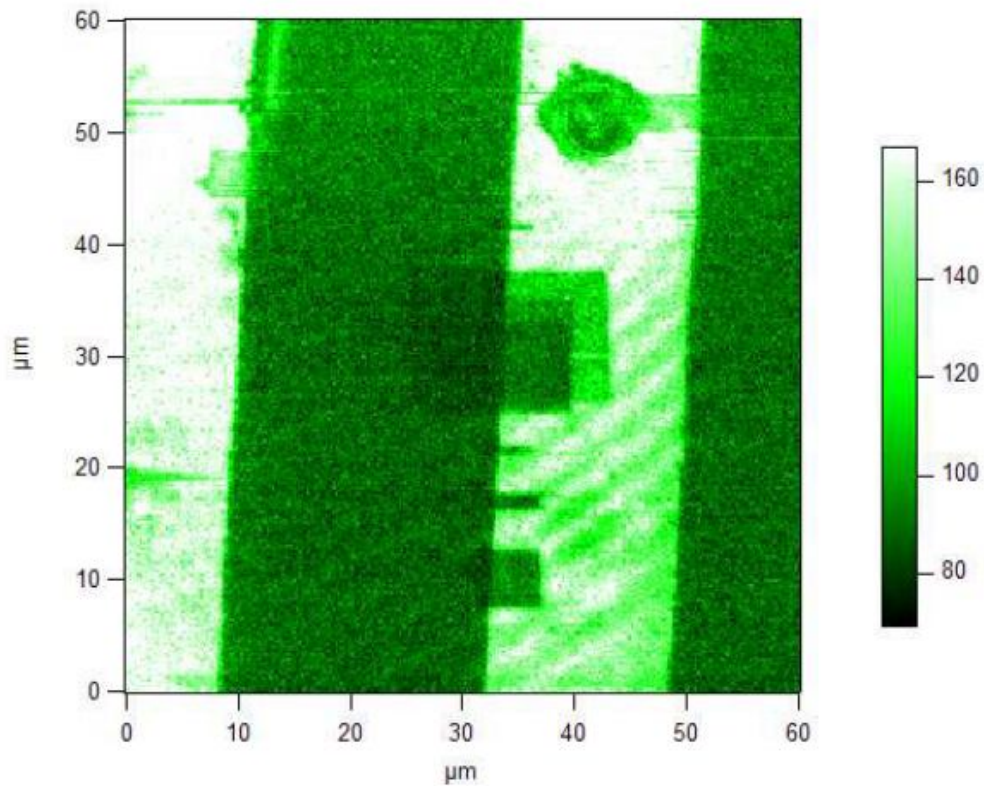


Figure. 1.5 SNOM image of Poly-L-lysine Stripes. In this picture a Fluorescence image of microcontact printed Poly-L-lysine stripes is shown. The left scale denotes counts per pixel. Excitation wavelength 488nm and the emission acquired with a FITC filter. Note that, local illumination as well as confined bleached regions were patterned. The photomultiplier tube allows photon counting in extremely low light intensity levels such as bioluminescent samples.

In the next section of this chapter, supplementary optical setups which allow diverse optical **imaging modes** will be discussed.

1.2 Convenient Optical Configurations for the Inverted Optical Microscope

Modern compound microscopes are designed to provide a magnified image in two dimensions which can be focused axially in successive focal planes, allowing with this careful examination from the structural detail from the specimen in the sample in two and three dimensions.

In the following, different **optical microscopy illumination techniques and fluorescence methods** with specific interest in fluorescence modes and their advantages will be discussed.

1.2.1 Phase Contrast and Epi-fluorescence

Presented in figure 1.1, the Olympus IX71 Inverted Optical Microscope is built for life cell imaging given that it is capable of manipulating near infrared (IR) wavelengths in addition to conventional visible spectrum. It provides access to the application of new fluorochromes being developed for live cell experiments which allow low photo-toxicity in reaction to light. It is also an instrument capable of efficiently detect faint fluorescent signals optimizing multicolor observation.

One of the most popular **microscopy illumination techniques** on which this microscope is capable of working, is phase contrast. This technique provides a well defined image of the object being observed in comparison to bright field images (see fig. 1.6).

a) Images missing!!
I'm taking them right now!

b)

Figure. 1.6 Different optical microscopy illumination techniques. This image shows a) a bright filed image and b) a phase contrast image of the same sample at the same

place taken one, right after the other. Osteoblastic cells from C2C12.

Transmitted **bright field illumination** is one of the most useful and common techniques in optical microscopy. It is ideal for fixed, stained biological specimens and other types of samples having high natural absorption of visible light. ~~Specimens such as living cells are virtually invisible given the way in which the light is transmitted through them.~~ Light passing through the sample undergoes a change in the amplitude and the phase of the waves (~~depending on the type of specimen~~); however, small changes in either one (due to differences in absorption, thickness and refractive index between the specimen and its surrounding medium) ~~are hardly detected by the human eye. Therefore, in many specimens that are unstained or still living, the contrast is so poor that bright field microscopy is incapable of rendering the specimens visible, despite the ability of the objective to resolve fine detail.~~ These specimens must be imaged with contrast-enhancing techniques, such as phase contrast, oblique illumination, differential interference contrast (DIC), darkfield, Hoffman modulated contrast (HMC), or Rheinberg illumination [Miller, 2009].

Phase contrast illumination takes advantage of having minimal differences in the refractive index among the cellular components, the intracellular media, the cellular wall and the aqueous media surrounding the cells to produce contrast between these similar transparent specimens.

~~This technique employs a mechanism in which minimal variations in phase are produced by the diffraction of light passing through the sample due to a change in the refractive index [Otaki, 2009]. The working principle is as follows (see fig. 1.7): the sample is illuminated using partially coherent light, which is directed through a phase ring, this ring literally lets only a "ring of light" through to illuminate the sample. The waves can either pass through the sample un-deviated (resulting in direct light), or scattered (or diffracted) and retarded in phase by the structures and phase gradients in the specimen. All the light passing through the sample is then collected by the objective and goes through at the phase plate, which delays direct light by $\lambda/4$ and allows the scattered light to go through, and is this phase delay which enhances the contrast. The scattered light is made to interfere with direct light and as a result, a phase difference and interference are observed when the light is focused at the image plane to form the phase contrast image observed in the eye pieces. Refer to Appendix B to setup phase contrast in the lab microscope.~~

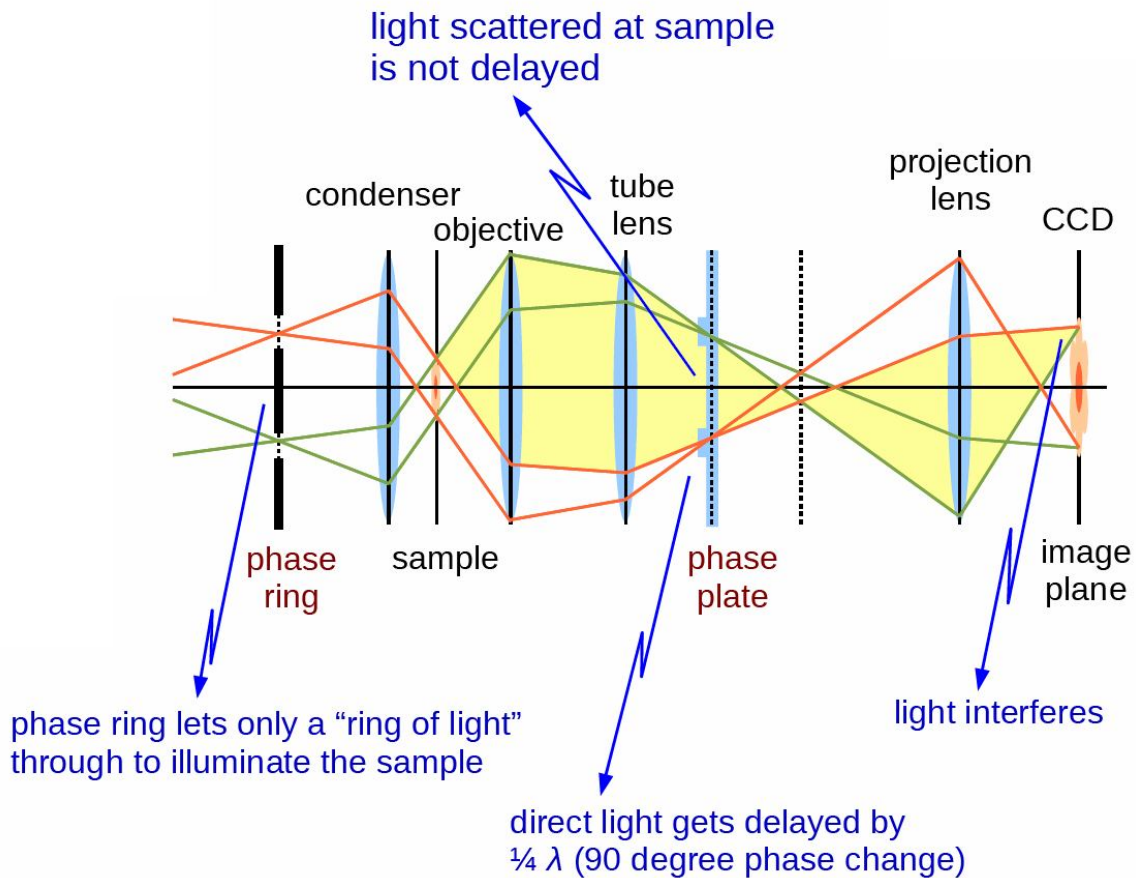


Figure. 1.7 Phase Contrast mechanism. This image shows how light coming from a source at the left side of the image is made interfere with a phase with respect to un-deviated light through the sample. These interfering waves proportionate corresponding changes in amplitude, which can be visualized as enhanced differences in the image contrast. Image authorized by Prof. Cris Luengo from Centre for Image Analysis (CBA) Sweden.

Another very common and useful optical microscopy technique which takes advantage of the ability of some organic and inorganic proteins to absorb and subsequently reradiate light is called epi-fluorescence, also identified as fluorescence. In our microscope, fluorescence imaging can be put into operation through the microscope optics. Different filters can be used in depending on the fluorochromes used. The band structure of the molecules imaged may require special excitation and emission wavelengths, therefore, different lasers have to be used to illuminate different samples (for more detail in the process read the following section).

The basic principle of **photoluminescence** resides in the ability of the electrons in the atoms and molecules of a material to ~~absorb enough energy to be removed from the potential energy barrier, jumping with this into an allowed excited energy level, and subsequently decaying back to the ground state, after having released some vibrational relaxation energy, releasing while decaying part of the energy absorbed in the form of light.~~ Therefore, the absorbed photon will have a higher energy and wavelength than the emitted photon [Young, 19686]. Therefore, starting with the spectrum of an element or molecule, one can identify the transitions accompanying emission or absorption of particular photons. Note that if the absorbed photon contains more energy than is necessary for a simple electronic transition, the excess energy is usually converted into vibrational energy.

In some atoms and/or molecules, the processes of **absorption** (excitation) and **emission** of electrons can sometimes be coincident with photons with wavelength around the visible spectrum. ~~Is in this case when they are useful as fluorescent probes (see table 1.1), which can be attached to other macromolecules (such as nucleic acids, lipids, enzymes or proteins) in which case they receive the name of fluorochromes.~~

Fluorochrome	Excitation maximum wavelength(nm)	Emission maximum wavelength(nm)
Blue fluorescent protein (EBFP)	380	440
Cyan fluorescent protein (ECFP)	434	477
Green fluorescent protein (EGFP)	489	508
Yellow fluorescent protein (EYFP)	514	527
Red fluorescent protein (DsRed)	558	583

Table. 1.1: Excitation and Emission Spectra of Fluorochromes commonly used in biology.

~~In the next section, TIRFM and the necessary modifications in the optics, which also allow working in Epi-fluorescence will be discussed.~~

1.2.2 Total Internal Reflection Fluorescence Microscopy

In this section an important implemented optical setup for our microscope, which allows working in **Total Internal Reflection Fluorescence Microscopy** (TIRFM) is described. TIRF represents one of the most useful and powerful fluorescence methods to work with. The most significant advantage from it over other fluorescent methods is allowing only a small fraction of the sample to be illuminated at the sample interface, providing with this great reduction of the background light from the bulk sample, thus enabling high quality images and the ability to detect single molecule fluorescence [Qu, 2004], and surface sensitivity, useful when certain surface adhesion proteins are labeled and expressed.

When working in fluorescence one can use the total internal reflection principle to excite the fluorescence a thin (~100-200 nm) optical section of the sample just above the sample-glass interface by using total internal reflection of the fluorescence excitation beam. Beyond the total internal reflection angle, the incoming beam of light is reflected back into the incoming light medium. However, a small part of the energy from the incoming light extends out of the interface to the external medium [Axelrod, 1990] which has a lower refractive index. This way, a so-called evanescent wave which power decreases exponentially (Eq. 1.1) is originated, giving place to only few hundreds of nanometers of the sample above the interface to be illuminated and excited to emit fluorescence.

$$I(z) = I_0 e^{-z/d} \quad (\text{Eq. 1.1})$$

The penetration depth, which establishes how far the light infiltrates into the sample, is expressed in the equation 1.2.

$$d = \frac{\lambda_0}{4\pi\sqrt{(n_i^2 \sin^2 \theta_i) - n_s^2}} \quad (\text{Eq. 1.2})$$

Where $I(z)$ follows an exponentially decaying intensity over the penetration depth d through the z direction, and d depends on λ_0 , the excitation wavelength, n_i the refractive index of the incidental medium, θ_i the

incidental angle and n_s , the refractive index of the sample. Note the characteristic distance for decay of the evanescent wave intensity is a function of the incident illumination angle, wavelength, and refractive index differences between media on each side of the interface, the greater the angle of the incidental beam is, the lower the penetration depth will be.

One of the most useful implementations of TIRF which allows other instrumentation such as micromanipulators, to be used is the Objective Lens Illumination (see fig. 1.8).

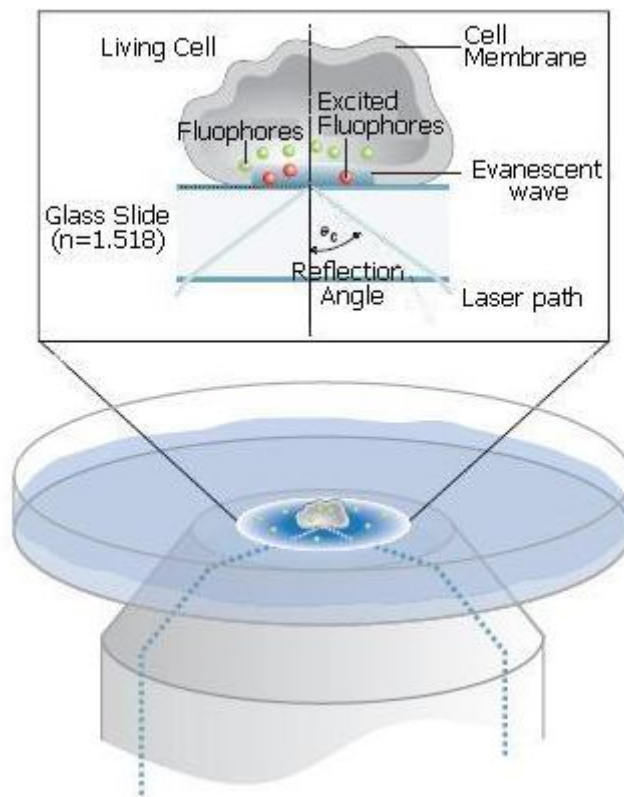


Figure. 1.8: Objective Lens Illumination. This figure shows the light path of the laser through the objective when a TIRF is put into operation. One of the major advantages of this method is the access to other instrumentation on top of the sample, which allows probing the sample enabling the study of different physical properties which may trigger a fluorescent signal.

Having a high numerical aperture (NA) lens greatly optimizes the amount of light collected by the objective, given that it is associated with the range of angles over which the system can accept or emit light. Thus, given the condition for total internal reflection and the definition of NA :

$$\theta_c = \sin^{-1}(n_s/n_i) \text{ where } n_i > n_s, \quad (\text{Eq. 1.3})$$

where n_i is the refractive index of the objective, n_s is the refractive index of the specimen, and θ_c is the critical angle, as for NA:

$$NA = n \cdot \sin(\alpha), \quad (\text{Eq. 1.4})$$

where NA is the numerical aperture of the objective lens and α is the ~~one-half~~ the objective ~~angular~~ aperture. Combining equations 1.3 and 1.4, we derive:

$$NA = n_i \cdot \sin(\theta_c) = n_s \quad (\text{Eq. 1.5})$$

Which translates into the fact that an immersion objective with high NA ($NA > 1.38$) is required to achieve total internal reflection since living cells typically have a refractive index between 1.35 and 1.37 [Liang, 2007].

In our microscope, a high NA Oil Objective: Olympus PLAPON 60X Objective for TIRF, this objective is specially designed for TIRF with a working distance of 1mm and an NA of 1.45 in $n=1.5126$ immersion oil. However, special modifications, ~~which will be described further on,~~ had to be ~~done to the setup~~ in order to work with TIRFM since there was no laser source coming in through the turret objective.

The TIRF setup consists basically of a laser coupled to an Optic Fiber, which injects the light into a fiber collimator from OFR, a 2X beam expander (produced by two lenses on the optical rail), a 45deg mirror to steer the beam in a tip-tilt mount. Up to here, the optics is mounted on the back of the fluorescence lamp port. The beam then enters the lamp port and is focused by a 150 mm focal length achromatic lens, which is placed to collimate and focus the beam in the Back Focal Plane (BFP) of the objective, ~~up to here epi-fluorescence can be achieved.~~ Now, by horizontally tilting the mirror the beam can be positioned off-axis on the BFP of the objective and, thus, shine on the sample at an angle high-enough for TIRF (see fig.1.9).

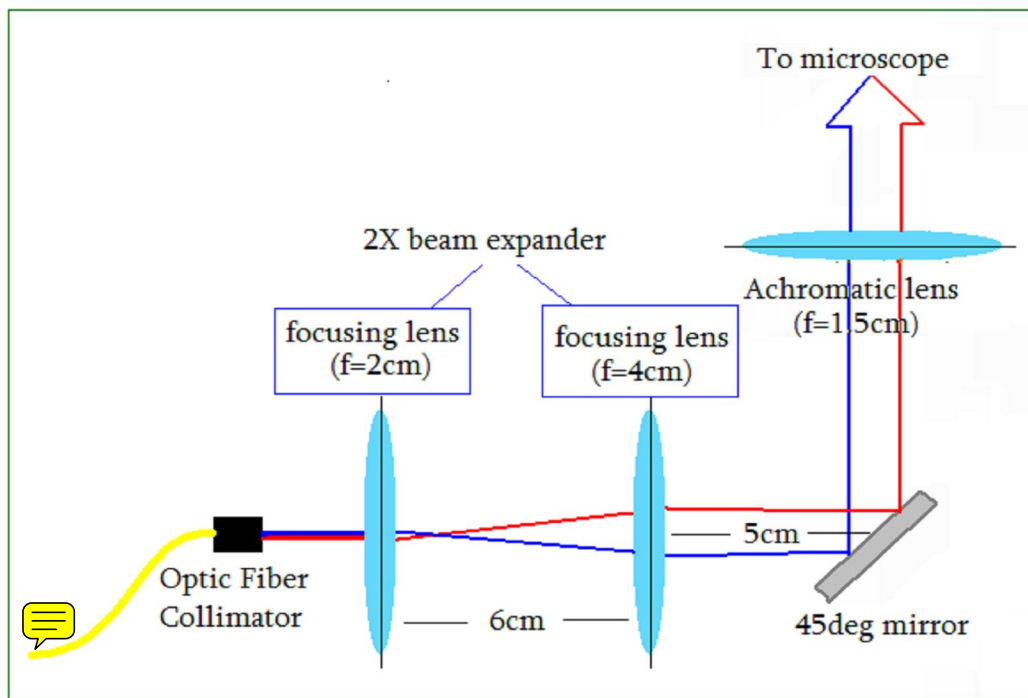
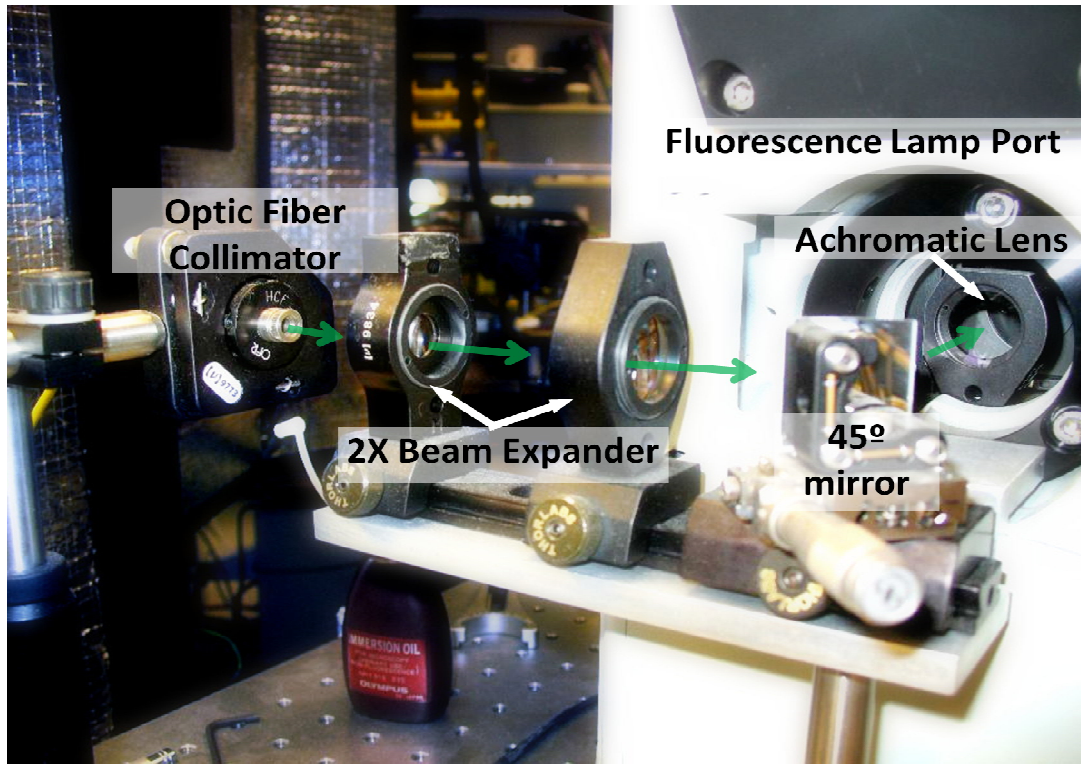



Figure. 1.9. TIRF laser optics on the back of IX71 microscope. This figure shows the path of the laser through the objective when either TIRF or Epi-fluorescence are put into operation. The green arrows in the top image show the laser path to the objective. The beam diagram and the lenses focal points are shown in the bottom image.

One of the major advantages of the Fluorescence methods in our setup is the easy access to other instrumentation on top of the sample, which allows probing the sample enabling the study of different physical properties which may trigger a fluorescent signal. 

Images in most of our fluorescence experiments, including the ones in figure 1.11, were taken using a modified Semrock FITC-3540B filter cube. It's FF506DI dichroic, reflects the 488 nm laser line and transmits sample light from 505 to 751 nm with $T > 20\%$. The emission filter was changed to a Chroma HQ505LP low-pass filter that transmits light at $\lambda > 505\text{nm}$. This modification allows seeing the full spectrum past the dichroic. The filter spectrum is shown in figure 1.10.

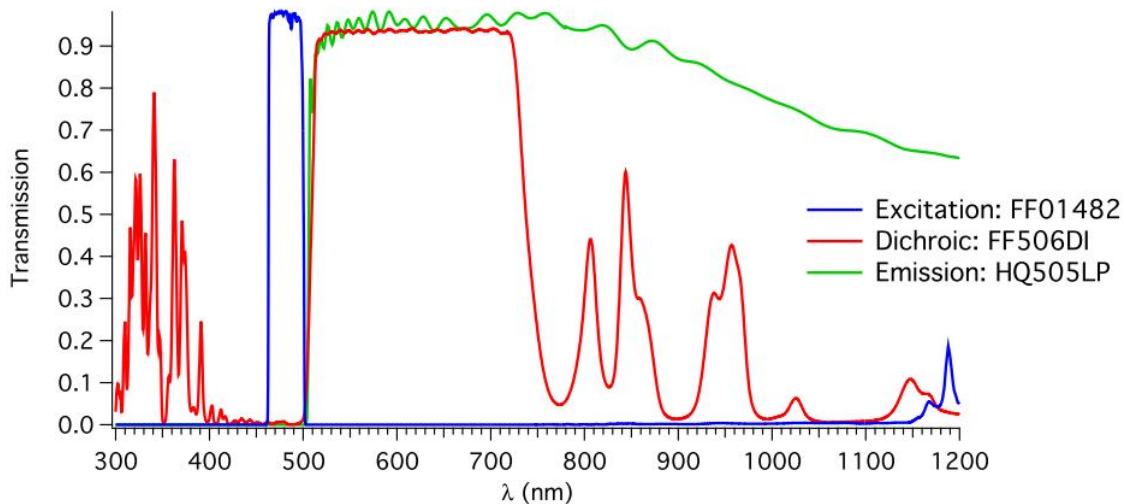
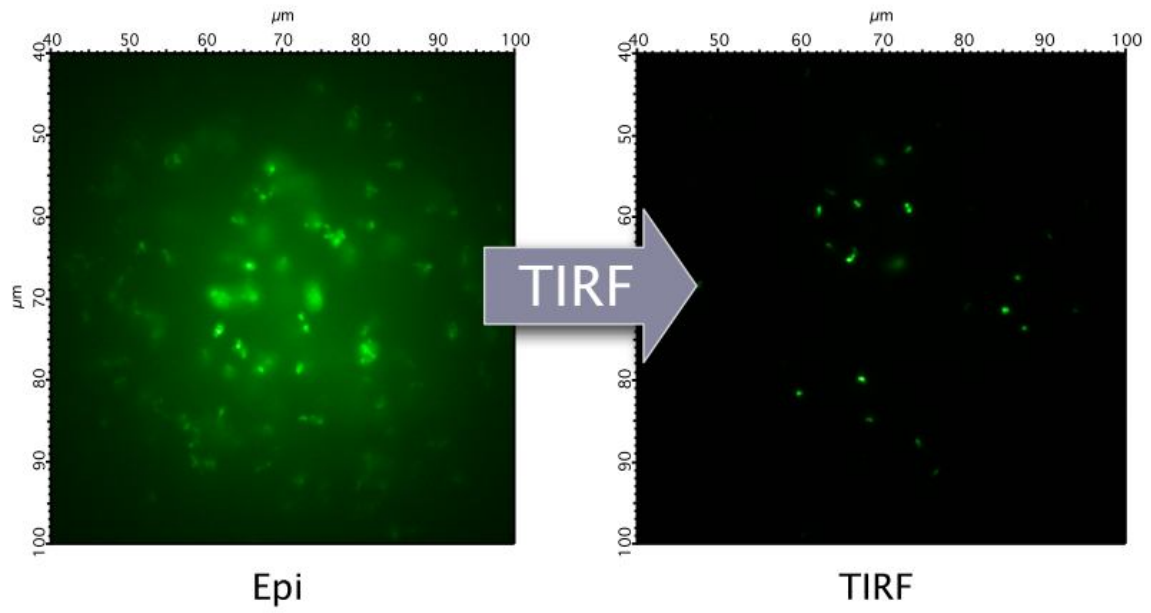


Figure. 1.10 Modified Semrock FITC 3540-B filter cube. This graph shows the filter cube Excitation and Emission spectra. When using it the sample is generally illuminated using the 488nm laser. The dichroic reflects the 488 nm laser line and sends it to the sample. The sample then emits and the dichroic transmits sample light in the 505 -751 nm range. The emission filter was changed to a Chroma HQ505LP low-pass filter that transmits light at $\lambda > 505\text{nm}$, which allows all the dichroic peaks to be transmitted.

Images in epi-fluorescence and TIRF are shown in figure 1.11. In order to compare the quality of the images and the subsequent reduction of the background light, as an effect of having a much better signal-to-noise ratio while working with TIRF ($S/N=16.5$ using epi-fluorescence, whereas $S/N=52.7$ using TIRF).



Epi $t_{\text{exp}}=200\text{ms}$ TIRF $t_{\text{exp}}=40\mu\text{s}$
 Figure. 1.11 Transition from Epi-fluorescence to TIRF, fluorescent microspheres

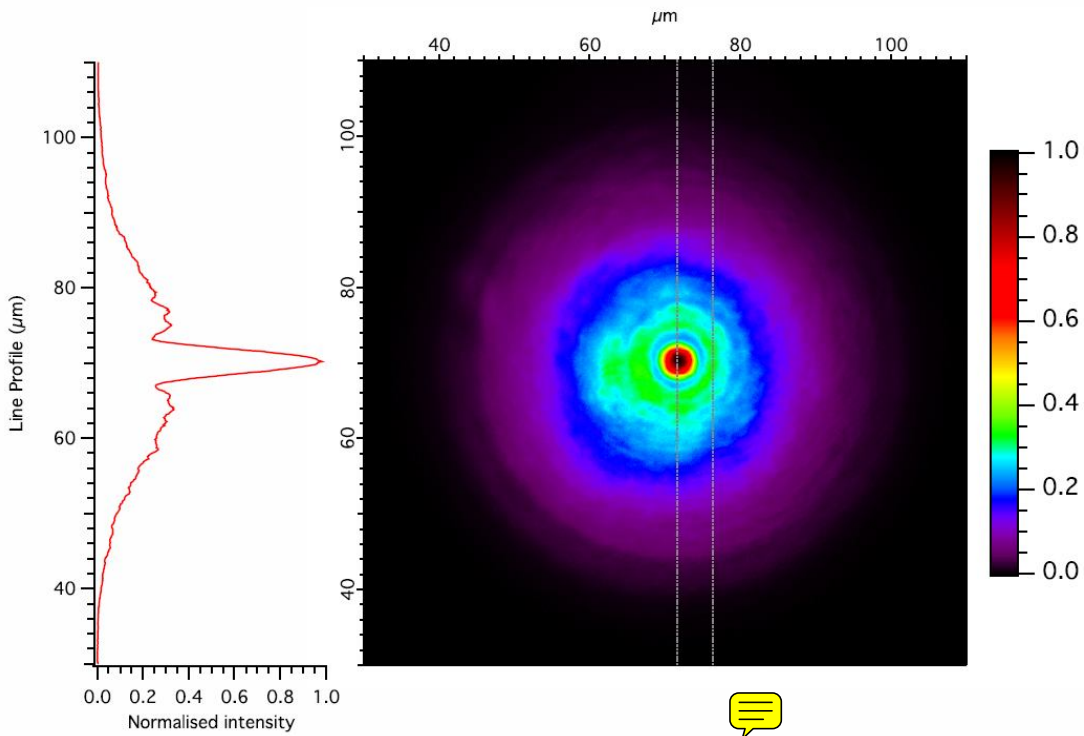


Figure. 1.12 Epi-fluorescence beam profile. The image on the right shows the circular beam shape. The central dotted line indicates the position of the line profile shown in the left side. There is a slight asymmetry on the left side of the beam, which may be due to a ghost beam resulting from partial reflection on the laser on one of the lenses. (Laser Power=171 μ W, t_{exp} =32ms)

Figure 1.13 shows the beam profile under TIRF. Going from epi to TIRF in a), and in b) at an angle close to the limit of the objective NA. In a), close to θ_{critic} for TIRF, the beam keeps its overall shape. However, the position of the maximum is slightly shifted towards where the beam is tilted. In b) the beam is considerably deformed. The maximum limit on the angle of illumination is the same as the maximum collection angle, which is controlled by the numerical aperture of the objective. Similarly expected in both cases, the beam is slightly widened, most likely due to the non perpendicular reflection on the mirror. By changing the mirror position one can illuminate the sample at increasingly large angles of incidence.

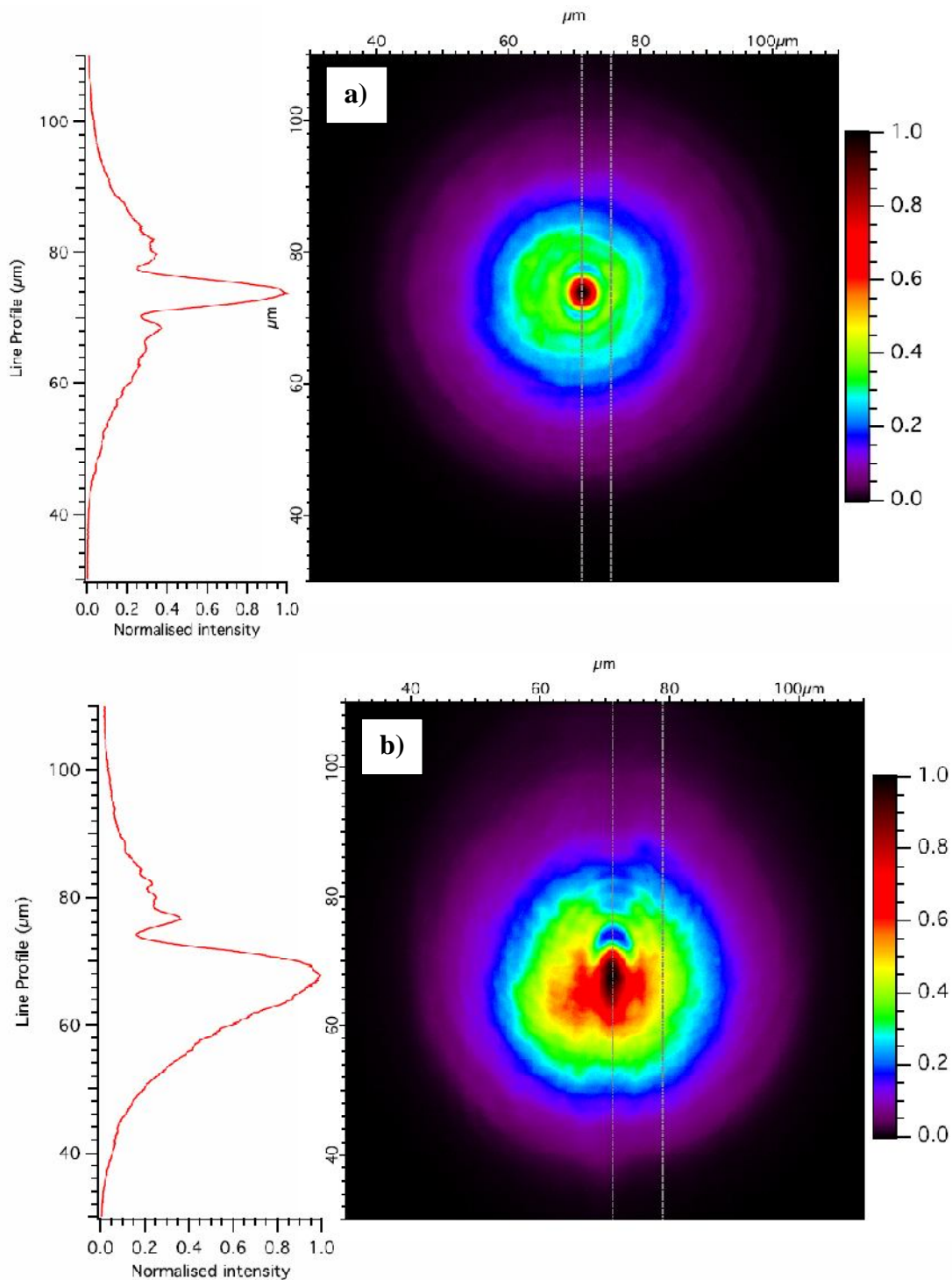


Figure. 1.13 TIRF beam profile. The image on the right shows the circular beam shape. The central dotted line indicates the position of the line profile shown in the left side. In a) In going from Epi to TIRF, the angle of the beam is close to $\theta_{critical}$ (Laser Power= $171\mu\text{W}$, $t_{exp}=16\text{ms}$). In b) In going from TIRF to the limit of the objective's NA (Laser Power= $58\mu\text{W}$, $t_{exp}=60\text{ms}$).



The design and principle of this setup was taken from [Pagie, 2001]. The beam expander was additionally implemented.


It has been shown that with this setup, incident angles, which are sufficiently large to allow TIR are achievable and switching from epi-fluorescence to TIRF is easily attainable. Moreover, the penetration depth of the evanescent wave used to illuminate the sample on TIRF diminishes the effect of the background fluorescence and leads to improved images with very high contrast having a good signal-to-noise ratio (3 times bigger compared to Epi). The key advantage of TIRFM over Epi-fluorescence is the shallow penetration depth of the evanescent wave.


The modifications done to the microscope optics, allow us to work both in epi-fluorescence and TIRFM, however, in the case of epi-fluorescence a lamp configuration might be more useful when different wavelengths are required to illuminate the sample ~~and the laser profile does not provide uniform~~ illumination.

1.3 Environmental Control

Depending on the nature of the experiment a sample holder which works in combination with a closed fluid cell can be used in two different configurations. One of which allows to seal the sample ~~environment~~ from the outside environment, and another in which the fluid cell is used in an "open" configuration. ~~It is to mention that the~~ closed fluid cell allows fluids to be drained and/or washed, it is designed to hold gases or liquids either statically or as part of a flow-through set-up in a completely enclosed and sealed cell. The closed cell is sealed by means of a flexible membrane which mounts to the MFP-3D cantilever holder. The membrane allows the tip to move freely relative to the sample, thereby allowing for distortion-free scans. It is made to maintain seals up to 2.5psi of water pressure to allow pressurized fluid exchange. The advantage of the open configuration is that it is easier to use, since it allows full access to the cantilever, the fluid and sample at any time during an experiment, while being still effective in



minimizing the evaporation and contamination of the solution of the liquid biological medium used for biological samples. 

 In addition to the liquid environment of the fluid cell, the Bio-heater allows the temperature of the fluid to which the biological sample is exposed to be controlled within $0.1\text{ }^{\circ}\text{C}$ to the desired value above room temperature and below 80°C . Using the open fluid cell configuration (see figure 1.14) and the heater, the experiments with cells reported in this work have been carried out.

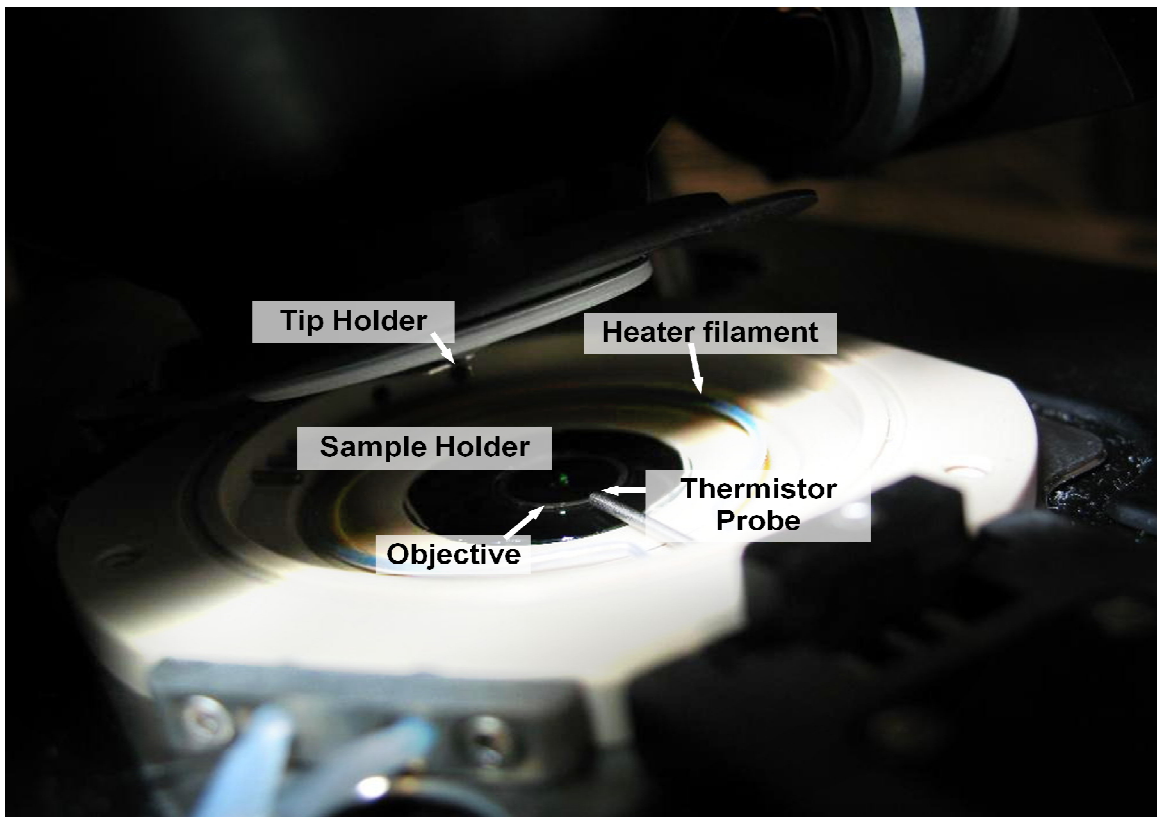


Figure. 1.14 Open Fluid cell configuration. This figure shows the Bio Heater stage where experiments with AFM MFP-3D Bio on cells are done. The heating system is composed by a thermistor probe, on the tip of which a temperature sensor is found. The heating filament and the thermometer to control the T . The fluid cell is made of peak and has magnets in the back, which allow attaching securely the fluid cell on to the AFM stage.

The following image (fig. 1.15) shows a sketch of the closed cell configuration, the only difference between the open and closed configuration is the employment of the closed fluid cell clamp, which prevents from gas and liquid leaks and holds the cantilever holder to the cell

dish. ~~It is to be mentioned that it has a capacity of up to 5ml before engaged.~~ The Petri Dish Holder allows cell samples to be cultured and imaged in Petri dishes up to 2mm thickness.

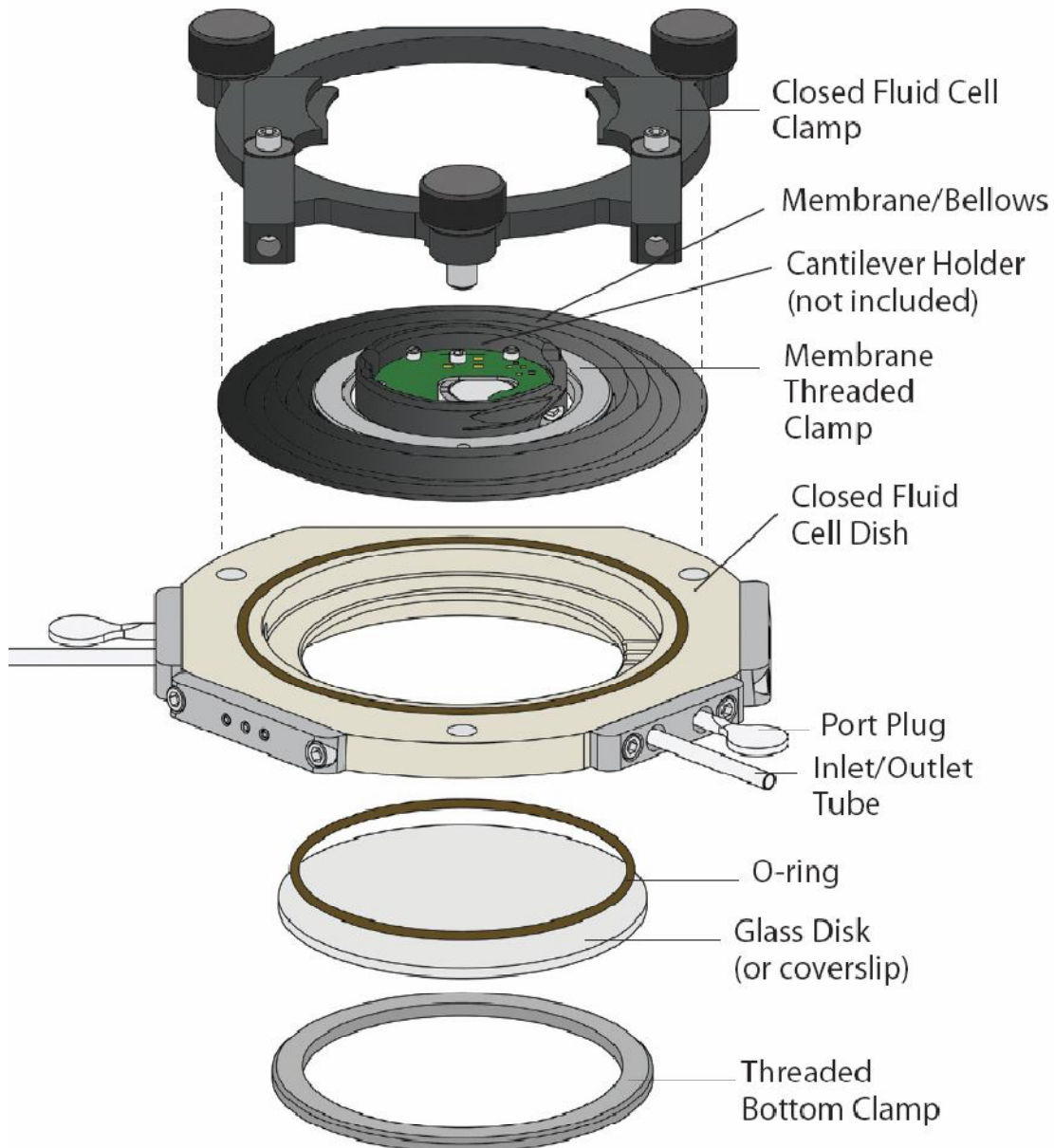


Figure. 1.15 Closed Fluid cell sketch. This figure shows the Closed cell parts. The fluid cell is made of a PEEK™ base that holds a 35mm diameter by 1mm thick glass disc for sample mounting. This glass disc can be replaced with special mounts that can hold 12mm or 25mm circular cover slips for high NA inverted optical microscopy.

All of the cell components can be easily removed and cleaned. The only materials that contact the fluid are PEEK, glass, silicone, FKM (Viton® equivalent O-ring material) and the cantilever holder. The entire cell (excluding the cantilever holder) can be sterilized in an autoclave.

In the next section, AFM and its experimental capabilities to resolve the surface topography and the forces related of different samples at the nanometer scale, as well as ~~the revision~~ of the forces applied will be explained.

1.4 Atomic Force Microscopy

~~In this section, some of the most used AFM techniques will be explained in order to elucidate the diversification of its capabilities. Both the force spectroscopy, which describes the interaction dynamics between the tip and the sample, and the imaging modes, will be discussed.~~

As suggested previously, the ability and precision of the AFM makes it suitable for experiments on mechanical properties of cells under physiological conditions. Different imaging techniques in AFM allow different features of the samples to be observed. In parallel, the origin and strength of the forces applied to the sample can be measured.

~~The high topographical resolution capabilities of AFM confer it as an essential instrument to understand the short and long range forces that result from the interaction between the surface and the sample. Great developments towards the study and manipulation of these forces have lead to different imaging techniques and supplementary tools to estimate mechanical properties of the sample according to its specific characteristics. Among the most used imaging modes in which the AFM can be operated, different levels of complexity and utility can be found. The AFM imaging modes which will be described in the following sections include: Force-Distance curves, which allow single indentation probing measurements, Force Volume, which permit different regions of the sample to be probed using single indentation, Contact mode, which lets to raster the rip over the sample as it is scanned and is useful for friction measurements, Tapping~~

mode (also known as AC-AFM), which basically taps the tip on the sample preventing from the appearance of lateral forces that usually appear while imaging in contact mode, and Non-Contact mode (NC-AFM) which is the most sensitive technique of all, it allows to select the regime (attractive or repulsive) within the force potential above the sample.

As will be discussed in further detail in the following sections, depending on the sample qualities and central events or features to observe, different tip-sample forces can be selected in order to extract different properties from the measurements by selecting the adequate tip and mode to work with.

1.4.1 Force Spectroscopy

One of the major advantages of AFM, other than imaging, is ~~the~~ Force Spectroscopy which allows a direct measurement of the tip-sample interaction forces by measuring the cantilever deflection as the tip approaches and retracts from the sample moved by the piezo electric translator in a so called **Force-Distance curve** (F-D curve). In this type of static measurement, the cantilever deflection (vertical bending, d) is recorded as a function of the piezoelectric scanner displacement (z). The cantilever deflection is converted afterwards into force (F) using Hooke's law: $F = k \times d$. When the rate of the increasing force (loading rate) is varied during an experiment, one can get an insight into the mechanical and molecular processes in the sample and their time scale relation.

Various features, such as long and short range contributions ~~may~~ be distinguished from the force curve, ~~resulting from the tip-sample interaction forces~~. At long range, the force experienced by the tip is zero (out of contact). As the tip approaches to the surface, the cantilever bends upwards due to repulsive interaction (electrostatic, hydration or steric forces) until the tip jumps in to contact due to short range van der Waals forces and is then repulsed again by Pauli forces until the maximum triggering force (or deflection) is reached and the cantilever retracted observing some adhesive forces due to impurities or water in the surface of the sample. [^]

The force resolution of the AFM depends on the setup as will be discussed in the next chapter, but is in general, [^] limited by the thermal noise of the



cantilever, which in turn in a well designed microscope, is determined by its spring constant. In addition, the quality factor (Q) and the measurement bandwidth ~~can also substantially contribute~~ [Viani, 1999]. Therefore, for single-molecule measurements, best results are generally attained with cantilevers exhibiting small spring constants and short lengths, because they exhibit lower force noise.

When the sample's surface is soft compared to the lever spring constant, as happens with most biological samples, the force applied by the cantilever will also induce a surface deformation (indentation) in the sample, which will increase gradually and non-linearly, in comparison to the hard substrate. These forces start at the contact point and follow up to the triggering force, after which the cantilever retracts. During the retraction regime, a viscoelastic response is generally observed since there is hysteresis between the approach and retraction curves most of the times. Adhesive forces appear as negative forces with respect to the zero-force baseline deflection and can indicate some molecular pulling events (see figure 1.16).

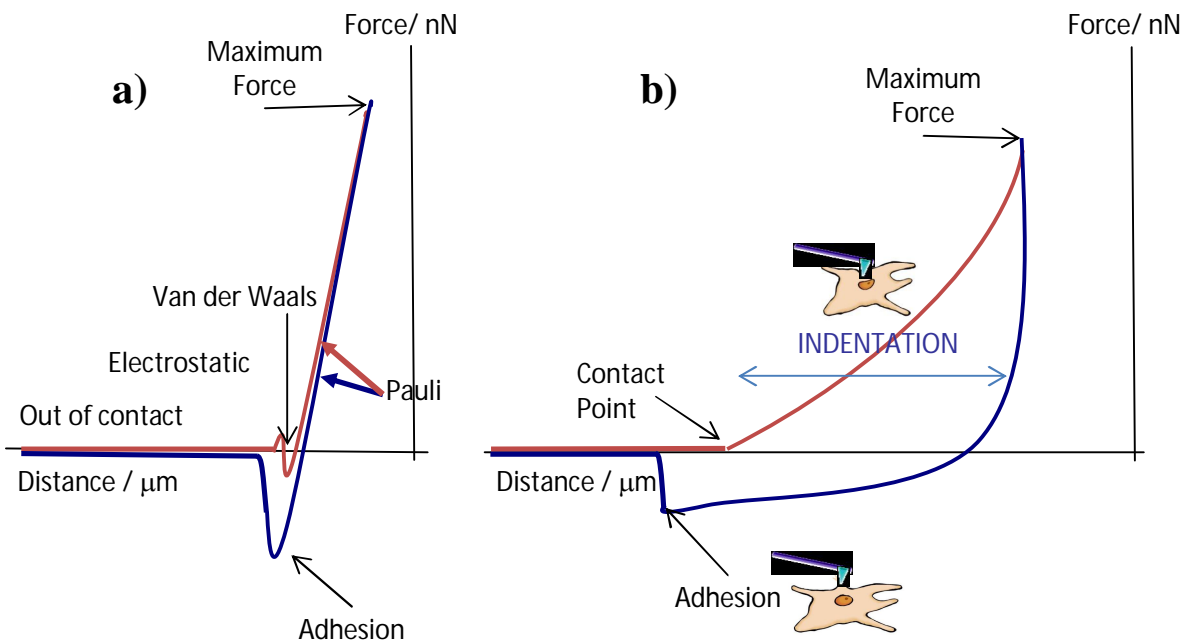


Figure. 1.16 Force-Distance curves. These figures represent FD curves both in hard substrate and soft biological samples. In **a)** the different long and short range forces are labeled. After contact, the cantilever is mainly deforming until the trigger point is reached. Since the tip is not indenting in the sample, a linear behavior is observed after the van der Waals forces appear, and is mainly Hookean. In **b)** the tip is indenting a cell, after the contact, ~~formerly the electrostatic interaction is suppressed, and afterwards~~

indentation behaves non-linearly due to sample deformation. In both cases adhesion forces can be observed.

By means of a F-D curve, one can get an idea of the force applied to the sample, the Young's modulus of the material can then be calculated depending on the end slope, shape and movement state of the cantilever [Kopycinska-Müller, 2006].

Although there are different models to describe the mechanisms of the tip-sample contact, all of them measure the local stiffness, and from it, the elastic properties of the sample can be inferred using a contact mechanics model. Consequently, all these models as well as other AFM contact techniques, must deal with the challenges of a nano-scale tip-sample contact. One of the most common and simplest models to interpret the F-D curves is the Hertzian model, which assumes that for a linear, elastic, isotropic and homogeneous sample of infinite thickness indented by a rigid, non-adhesive tip of known geometry with small applied static loads by [Schwarz, 1997], the contact mechanics is described by [Johnson, 1978]:


$$F_s = \frac{4ER^{1/2}}{3(1-\nu^2)} \delta^{3/2}, \text{ for spherical indenter of radius } R \gg \delta, \text{ and} \quad (\text{Eq. 1.6})$$

$$F_c = \frac{2E \tan(\theta) R^{1/2}}{\pi(1-\nu^2)} \delta^2, \text{ for conical indenter of half opening angle } \theta \quad (\text{Eq. 1.7}).$$

Where E and ν represent the Young's Modulus, which can be described as the elastic property of a solid undergoing a tension or compression pressure to change its dimensions in the same direction of the force applied ([stress/strain]=[Pas]), and the Poisson's ration of the sample, the induced bulging at the sides of the material; the ratio, of the contraction or transverse strain (perpendicular to the applied load), to the extension or axial strain (in the direction of the applied load) when a sample object is stretched or compressed, and is in general a number between -1 and 0.5 being the later the upper related to incompressible materials (such as cells [Yamada, 2000]). The indentation is the z-piezo motion relative to the contact point defined as $\delta = z - d$, where z is the z-piezo motion and d is the deflection signal relative to the non-contact deflection. If the indentation region is fitted its appropriate description (given the geometry of the

indenter), the Young's modulus can be determined. It is to mention that for small indentations the tip geometry is generally approximated ~~to the spherical indenter.~~

Alternative models perhaps more suitable for biological samples, which attempt to soften the Hertzian model assumptions, have been developed in order to study the indentation mechanics in a more realistic situation. In particular, it is usually necessary to correct for adhesion, ~~since it is related with hysteresis between the tip liquid surface interactions and is caused by the different degrees of hydrophobicity and attractivity of the surfaces in the media and by the different solubilities of these molecules in the present liquid~~ [Weisenhorn, 1992]. Viscous forces can also introduce drag and the analysis of the data through the Hertzian model can ~~result~~ highly convoluted [Radmacher, 1996]. Some models can be found in the following references: [Dimitriadis, 2002], [Vanlandingham, 2005], [White, 2005], [Attard, 2007] [Shulha, 2004], [Tsukruk, 1998], [Costa, 1999].

While F-D curves provide a method for determination of local mechanical properties, the study of cellular mechanics often requires the characterization of the distribution and variance of these properties over the surface of the cell or the 3D structure laying in the surface. In this case, **Force Volume Imaging** produces a collection of F-D curves over an area of the sample's surface, therefore, providing a mechanical property profile in addition to topography map of the sample in place as seen in figure 1.17 (image courtesy of Dr Grutter's group [Smith, 2005]). These maps ~~consent~~ the enhancement of the mechanical response in localized spots ~~on the sample being able to distinguish topography from material properties~~ [Grandbois, 2000]. 

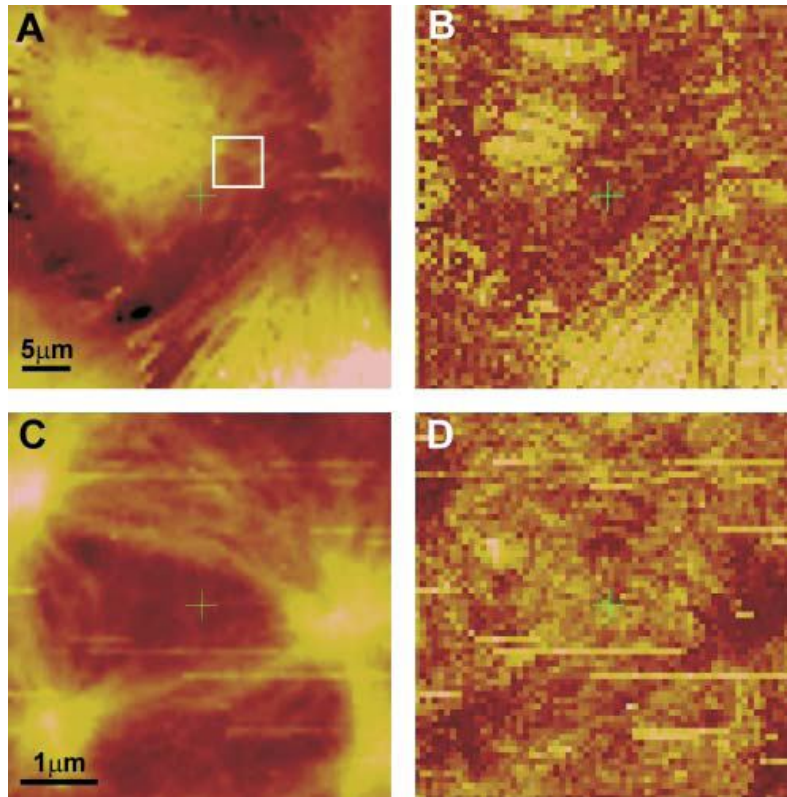


Figure. 1.17 Force volume height. (A, C) and elasticity (B, D) profiles of a confluent culture of rat tracheal smooth muscle cells using a constant maximum applied force of ;0.4 nN (height color scale spans 1 mm in A and 0.3 mm in C; dark is stiff and light is soft in the elasticity maps). These images reveal a stiff fibrous network that is highly nodal and spans the entire cell, although the nuclear region appears to provide a very soft background (large light region in the top left quarter of B). The higher resolution images in C and D clearly identify the nodes as well as their interconnecting fibers as the structures of mechanical rigidity within the cell [Smith, 2005].

~~Using this method, the nature of the interaction can be deduced through analysis of individual F-D curves. Normal forces are measured; therefore there is no thermal drift of the lever, as there is, in other imaging modes. This will be furtherly discussed in the next section. Lateral forces are therefore eliminated. It is to point out that the F-D curves can be made as well using other Dynamic Modes, such as tapping and non-contact mode, the analysis of the force will therefore be different as will be specified further on when necessary.~~

In the following part, different topography imaging modes will be discussed.

1.4.2 Imaging modes in AFM

The interaction dynamics between the AFM tip and the sample, plus the ability and the precision of the instruments make AFM a potent technique for studies of mechanical properties of cells under physiological conditions. In this section the most used imaging modes of AFM: Contact Mode (which is static), Tapping and Non-Contact Modes (which are dynamic), will be discussed.

Contact Mode

This mode responds using the force applied by the tip into the sample as feedback, the modulation of the z piezo extension is determined by the force applied, which is calculated from the cantilever deflection. The tip deflection data will stack to form a tip convolution image which we will interpret as the topography and the tip-sample forces.

This imaging mode often causes drag of not well adhered objects in the sample and harmful lateral forces, and is therefore not as widely used in life samples as the dynamic modes.

Following the force calculation related to static F-D curves follows the Hookean model discussed in the previous section. The force applied to the sample is calculated from the deflection of the cantilever in this mode. The fig. 1.18 shows a Au Triangles sample imaged in Contact mode underwater.

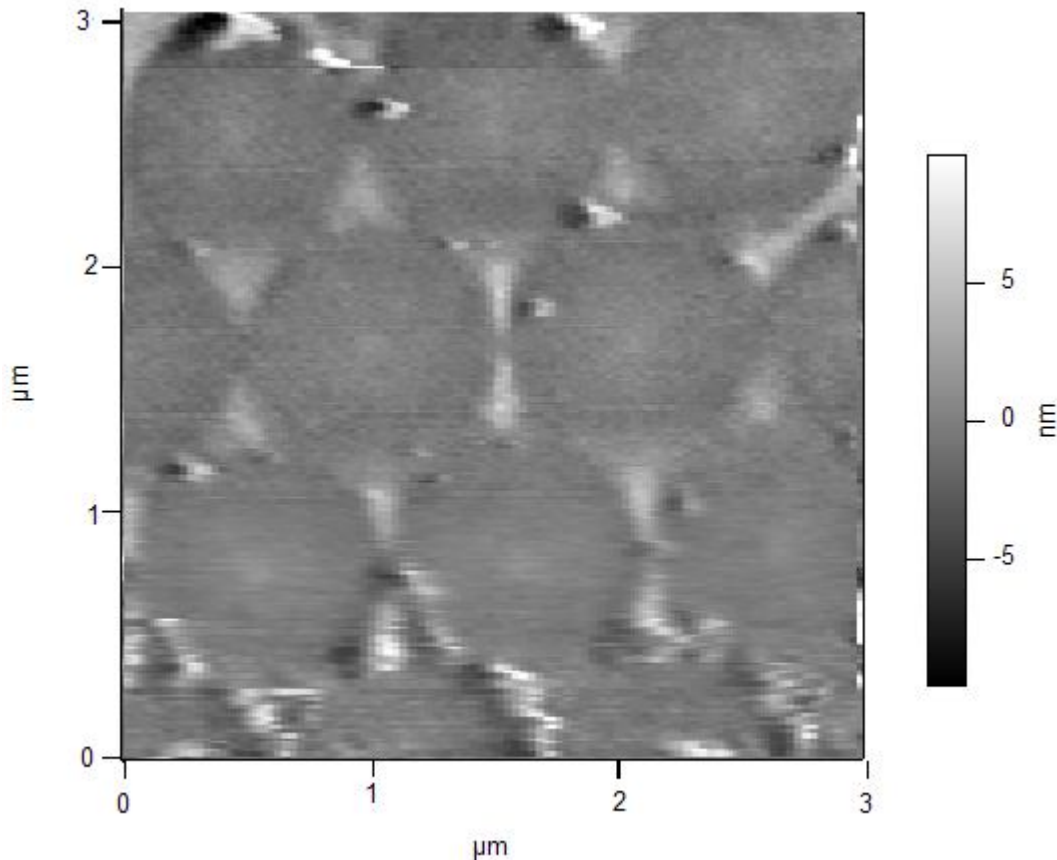


Figure. 1.18 Au Triangles sample in Contact mode. This Contact mode image taken underwater shows the surface topography of a self assembled array of polystyrene beads in glass, evaporated with Au, after Au deposition, the polystyrene beads were removed and only Au triangles remained. Normal load applied on the sample: 200 nN.

Tapping Mode

~~As an alternative to contact mode, and~~ in an effort to reduce the lateral forces caused by the raster scanned tip over the surface, ~~an oscillating cantilever~~ may be used in a dynamic imaging mode, ~~this is the case of this mode (tapping) and the following (non-contact).~~ In oscillatory motion in general, the amplitude and the frequency determine the characteristics of the wave, therefore, when these parameters are used as the modulation constraint, two new methods to apply, study and sense the tip-sample interaction forces emerge: amplitude modulation (AM or Tapping) and frequency modulation (FM or Non-Contact) detection.

In tapping mode the cantilever is excited by an external driving force with constant amplitude at a fixed frequency, usually near or on the free resonance. The resultant cantilever amplitude and phase are detected. When the amplitude of the oscillation starts to decrease (see fig 1.19), the cantilever is often partially oscillating off the sample; the amplitude detected indicates that a portion of the cycle of every oscillation, the cantilever is in or off contact with the sample. In this imaging mode the triggering parameter is the partial free amplitude, and it is kept constant by modulating the tip sample separation by modulating the z piezo extension while the sample is scanned under the tip [Schirmeisen, 2004].

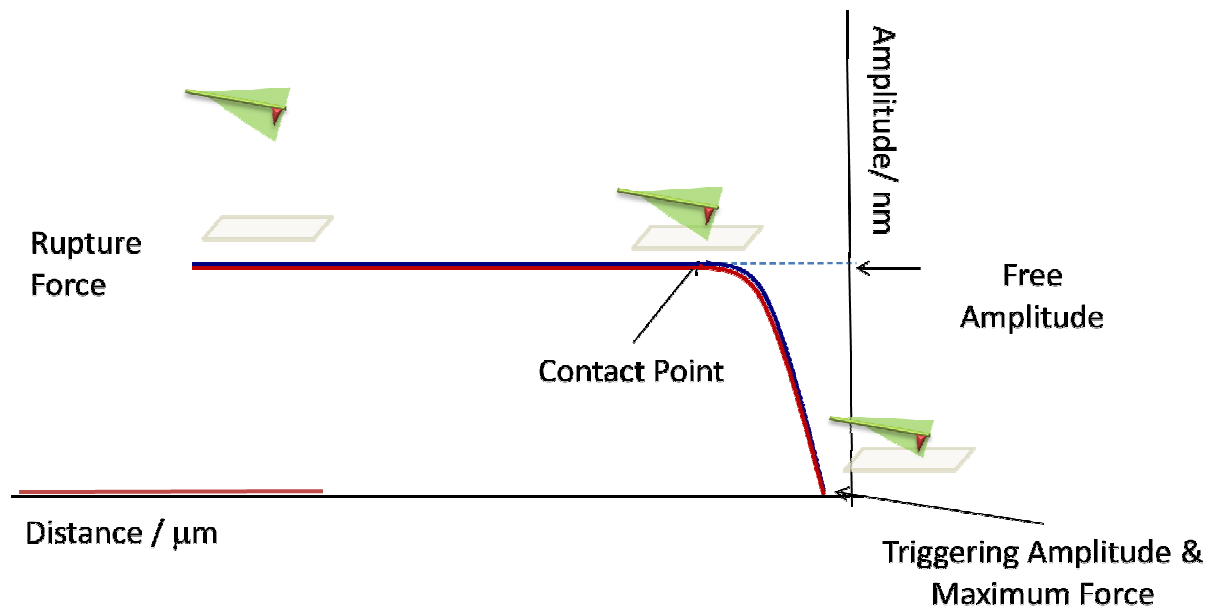


Figure. 1.19 Tapping Mode Force-Distance curve. This figure represents a FD curve in tapping mode. After the contact point the cantilever amplitude decreases until the trigger point is reached.

In order to operate in the AM mode, a sharp resonance is necessary to achieve stability and low noise operation. The behavior of the system with Low Q factors offers a fast response, but low sensitivity, while high Q factor values offer higher sensitivity but restrict the bandwidth, thus, producing a slow response since steady-state amplitude has to be reached [Albercht,

1991]. When measurements are performed in physiological solutions, the force sensors are immersed in water which strongly dampens oscillations and thus decreases the Q factor, decreasing in consequence the sensitivity.

In order to estimate the force applied to the sample for this mode of operation, the two general analytical relations for the amplitude, phase, and interaction forces are given by:

$$-\frac{F}{2} \sin(\theta) + \frac{A}{2} (k - m\omega^2) = \int_0^\pi \frac{d\tau}{\pi} F_c(z + A \cos(\tau))$$

$$\frac{1}{2} \left(\frac{F}{A\omega} \cos(\theta) - b \right) = \int_0^\pi \frac{d\tau}{\pi} \Gamma(z + A \cos(\tau)) \sin^2(\tau)$$

where A and θ are the amplitude and the phase respectively, F_c is the conservative term of the force, which depends only of the distance z and Γ is the effective damping coefficient, and the variable of integration τ , is the angular position of the cantilever at any given time, i.e. the force is integrated over one full cycle of the cantilever oscillation [Lee, 2006].

Even though the dynamics of the AFM probe for given tip-sample interactions is complicated, it has been successfully understood by analytical and numerical methods, describing the bistable and hysteretic behavior of the tip in proximity to the surface [Garcia, 2002]. Nonetheless, there does not still exist a complete understanding of the experimental measurements mainly due to the nonlinearity of the motion. Figure 1.20 shows an AC mode topography image of the Au triangles sample in glass.

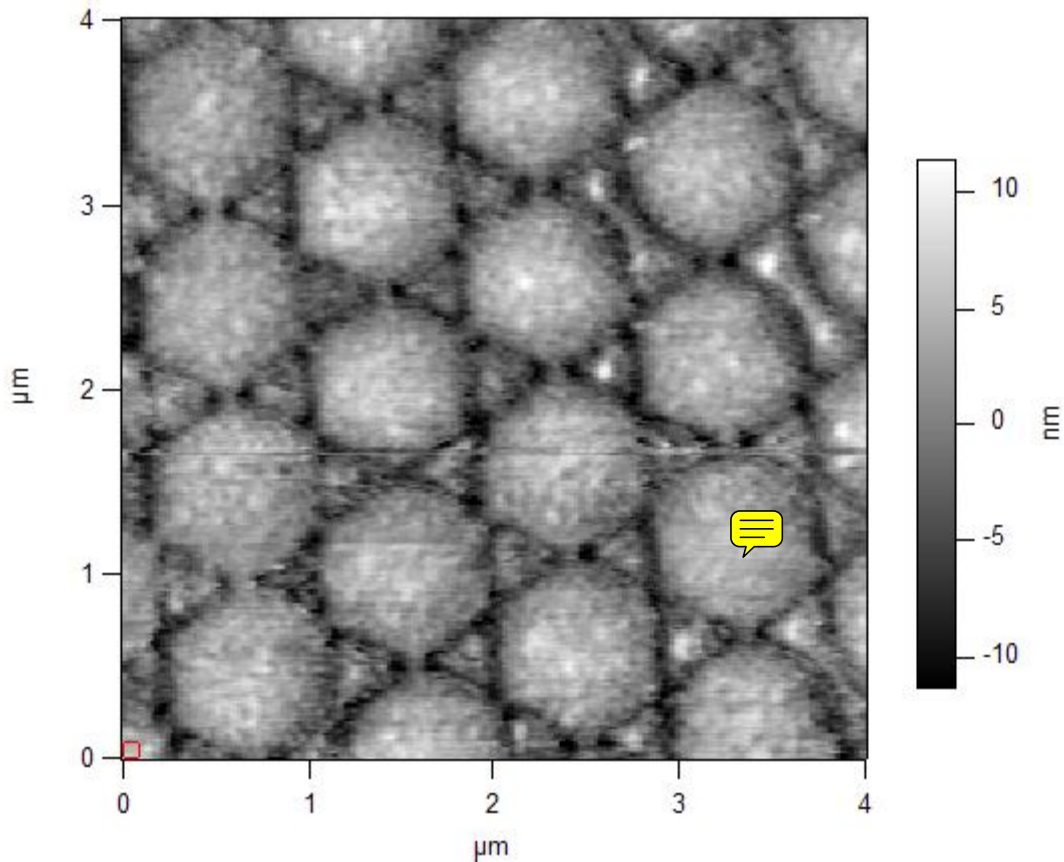


Figure. 1.20 Au Triangles sample in Tapping mode. This AC mode image taken underwater shows the surface topography of the same sample and place as Au triangles in figure 1.18. $F_{res}=6\text{kHz}$, $Q=8$.

Non-Contact Mode

Alternatively, when an oscillating tip approaches the sample, the frequency will shift. This way, by setting an excitation on the frequency, changes in frequency due to the tip sample "contact" will be detected. The frequency shift will then be the feedback parameter. This mode is the most sensitive and less destructive of all, since the sample will start to induce a frequency shift in the lever even before the lever touches the sample, i.e. in the attractive regime, where the Electrostatic and van der Waals forces can be resolved. As of here, this mode is called "Non-Contact (NC) mode" [Martin, 1987].

~~In this mode, the cantilever and the tip are oscillated on the surface and due to the tip-sample interaction, the resonance frequency and the tip-sample interaction change. In analogy to this, we could think of a coupled spring system in series, where the first spring bonds tip and sample, and the second bonds the tip and the cantilever. Changes in the frequency of oscillation of one will cause frequency changes in the other one.~~

In order to estimate the force applied to the sample for this mode of operation, considering the amplitude of oscillation is small compared to the to the decay length of the force:

$$\frac{\Delta f}{f_0} kA = \int_0^{2\pi} \frac{d\phi}{2\pi} F(\bar{z} + A \cos(\phi)) \cos(\phi) \quad \text{}$$

where Δf is the frequency shift, f_0 is the resonant frequency of the cantilever, k is the spring constant of the cantilever, A is the amplitude of the oscillations, and the variable of integration ϕ , is the angular position of the cantilever at any given time, i.e. the force is integrated over one full cycle of the cantilever oscillation. Indicating the frequency shift is proportional to the force gradient.

~~It is to mention, that~~ additional features and instrumentation for this imaging mode, will be discussed in detail as required in the following chapters. As an example image, ~~the~~ fig. 1.21 shows a glass surface scanned in NC mode underwater.

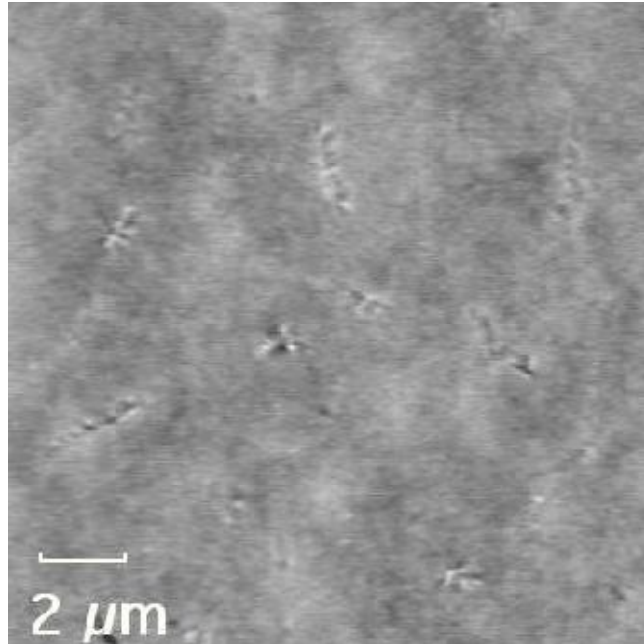


Figure. 1.21 Glass surface in NC mode. This NC mode image was taken in air with amplitude of 10 nm, frequency shift of +64 Hz, resonance frequency of 39.212 kHz, and a Q factor of 60. The vertical scale is 3 nm from black to white.

~~Intended~~ for oscillations in which the amplitude is comparable to the decay length of the force, [^]the interaction results [^]more complex ~~and the expression for it~~ can be found in [Guggisberg, 2000]. In order to convert the frequency shift to force, different methods are discussed in the following references: [Dürig, 2000], [Giessibl, 2001].

~~In order to enclose the discussion along~~ this section, the following chart (Table 1.2) shows a comparison between the different imaging modes.

AFM Modes	Static	Dynamic	
	Contact	Amplitude Modulation (Tapping)	Frequency Modulation (Non Contact)
Advantages	The force is proportional to the deflection	Reduces harmful lateral forces The interaction is reduced to the portion of the oscillation Normal Forces can be quite large	Can achieve molecular and atomic resolution Lower forces can be applied, therefore it's less destructive Higher sensitivity Changes in f are instantaneously detected Thermal noise decrease when increasing Q Band width and Q are independent of each other The force calculation is moderately simple The attractive and repulsive regimes can be detected and used to work.
Disadvantages	Often causes drag of not well adhered objects in the sample and harmful lateral forces	Sensitivity depends on the Q and the Bandwidth Increasing Q restricts the bandwidth (response time increases), but improves the signal to noise ratio The force calculation is complicated Other modes of oscillation may appear	Instrument not commercially available in the bio-field and not yet applied to living cells in solution
	Sensitivity decreases in aqueous media because of the drag force in the cantilever		

Table 1.2. AFM Modes Comparison.

In conclusion, working in a dynamic mode decrease lateral forces, the interaction can be controlled reducing the destructive effects, however, other modes of oscillation may appear. N-C mode allows the oscillating AFM force sensor to operate over the sample with very low applied forces, thus increasing the resolution and the imaging speed in comparison to other AFM imaging modes and minimizing the drag caused by lateral forces [Albercht, 1991]. In order to operate in N-C mode, a sharp resonance is necessary to achieve stability and low noise operation, therefore, experiments using this mode are common in high vacuum systems, is also for this reason that the tips for dynamic modes are in general stiffer than contact mode tips. However, when measurements are performed in physiological solutions, the cantilevers are immersed in water which strongly dampens oscillations and thus decreases the mechanical Q factor in liquid, which can lead to a substantial increase of noise [Fukuma, 2005]. In chapter 4 a "Diving Bell" setup will be discussed and results of its implementation will show to improve the Q factor in physiological solution, therefore increasing the sensitivity and the imaging capabilities in liquids.



The experimental methods elucidated in this chapter establish the basic elements applied for the study of cells in physiological environments. In the next two chapters, additional instrumental features to further characterization of the microscope capabilities such as the noise of the setup and the ability to resolve single water layering close to a sample in Chapter 2, and the "Diving Bell" setup used to achieve high Q factors under liquids using home fabricated SNOM based cantilevers will be elucidated in Chapter 3. An example application of the microscope for biological samples through force spectroscopy in the study of bone cell mechano-transduction and signaling pathways will be exposed in Chapter 4.

Chapter 2

Noise in combined optical microscopy and NC-AFM: towards in-vivo hydration measurements

3.1 Noise characterization	3
3.2 Noise modeling	3
3.3 Hydration	3
3.3.1 Hydration measurements.....	3
4.5 Conclusions	12

Chapter 3

High Q Optical Fiber tips for NCAFM in liquids

4.1 Bent fiber probe fabrication	12
4.2 Diving Bell for Liquid Operation	12
4.3 NC-AFM set-up	12
4.4 High Q in liquid using the diving bell.	12
4.5 Imaging and force spectroscopy.	12
4.6 Conclusions	12

Chapter 4

Application to Biological Samples



Knowledge of the mechanical properties and molecular interaction between ligands and receptors, either on isolated membranes or on cellular surfaces is important in life sciences. Cells can sense mechanical stimuli through mechano-sensitive ion channels, receptors, or enzymes [Malek and Izumo, 1996], [Banes et al., 1995], [Sachs, 1998]. The mechanisms involved and downstream ~~of~~-events may depend on the type of stimulation and are likely to involve cell specific components [Vauquelin, 2009].

Atomic Force Microscopy (AFM) has diversified from ultra high vacuum to liquid, making possible experiments in cells and bio-molecules using high resolution imaging and force spectroscopy. The local interaction dynamics between the AFM tip and the sample, plus the ability and the precision of the instrument makes AFM a potent technique for studies of mechanical properties of cells under physiological conditions.

In this section a study of the signaling pathways resulting from mechanical stimulation of a single bone cell is presented. AFM force spectroscopy was combined with fluorescence to describe the phenomena observed. This work was done in collaboration with Dr. Komarova's lab from the Faculty of Dentistry at McGill University.

4.1 Characterization of Mechano-transduction in Bone Cells

Bone is a continuously remodeling living tissue that gives support to our body. It is formed mainly by cellular and mineral matrix components. During childhood and adolescence, there is an increase in bone mass. The bone health, the bone mass and the subsequent bone loss are important factors that determine the incidence in osteoporosis with aging. It has been suggested that by maximizing the Peak Bone Mass, reached after full growth [Bonjour, 1994] could be an important strategy in preventing osteoporosis in later stages in life [Hui, 1990].

Physical activity has been proposed as a major determinant of Bone Mineral Density as [Bass, 1998], [Suominen, 1993]. Different sporting disciplines result in a site-specific BMD increase that are supposedly related to the high and unusual strains created at certain sites during sports training by impact loading, muscle stress and gravitational forces [Morel, 2001].

Moreover, it is well known that significant bone loss occurs during human adaptation to long-duration spaceflight under microgravity, our understanding of the effects of microgravity on the bone resorption and formation remains unclear. Studies suggest, that portions of the human skeleton are subjected to large but transient mechanical loads in opposition to gravity during normal activities such as walking and lifting. Because of the fundamental importance of dynamic gravitational loading, it is reasonable to expect that the skeletal system would be especially sensitive to changes in gravity [Turner, 2000].

Due to similar reasons, long-term bed rest patients or patients experiencing any other kind of bone weight-bearing unloading experience intensified bone loss accompanied by BMD reduction and interference with the bone turnover (healthy growth and maintenance) process. In this sense, unloading of weight-bearing bones rapidly increases bone resorption, whereas bone formation decreases [Caillot, 1998], [Baecker, 2003]. This occurs due to the disequilibrium in the bone formation-resorption process performed by bone-forming cells, osteoblasts and bone-resorbing cells, osteoclasts, (a brief description of the function of each of the bone cells in

the turnover process is presented in Figure 4.1). For further detail please refer to [Collin, 1995].

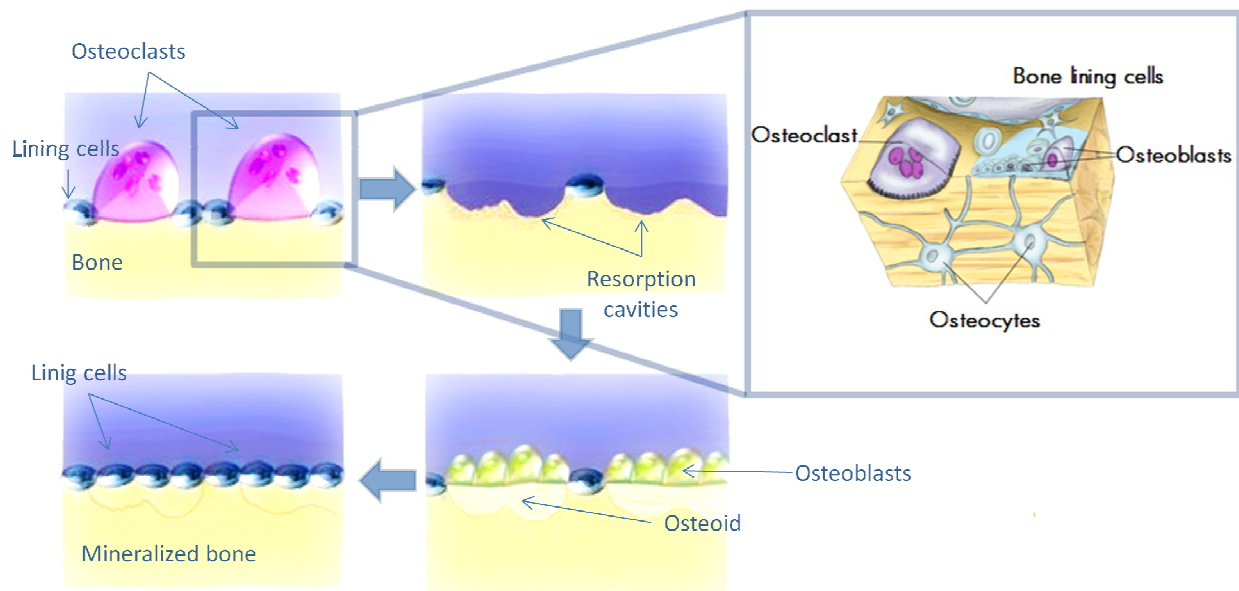


Figure. 4.1 Bone Cells Function in Bone Turnover. This diagram illustrates how bone cells function in healthy bone. The bone remodeling process begins when the cells lining the bone surface are activated to form **Osteoclasts**: (bone resorption/eating cells) large multi-nucleated cells that break down bone tissue by secreting acid, which dissolves the bone mineral to form resorption cavities. **Osteoblasts** (bone formation cells) are recruited to the resorbed bone and secrete osteoid matrix, an unmineralized ground substance, composed mainly of collagen, to form new bone matrix. These cells are found in areas of high metabolism within the bone. Over time, the osteoid matrix mineralizes to become bone. [Graaff, 1998]. Image published with permission from Medical Look.



Having recognized the fact that the skeleton adapts to its mechanical usage, the aim of this work is to elucidate how at the cellular level the distribution and magnitude of mechanical strains is communicated within and among bone cells. We modeled the mechanical stimulation at the single cell level and studied the mechano-transduction process to understand the signaling pathways through which a single stimulated cell can produce and induce calcium signaling, in the stimulated cell and in other neighboring non connected cells.

4.1.1 Bone Cell and Mechanotransduction

Due to the complex architecture of bone, the strain to which cells are subjected in vivo and the reaction pathways remain unknown. In some studies, it has been shown that cells can sense mechanical stimuli through mechano-sensitive ion channels [Sachs, 1998], integrin receptors [Banes, 1995] or tyrosine kinases [Malek, 1996]. The exact mechanism implicated in mechano-transduction and the downstream events may depend on the type of stimulation and is considered to relate to different cellular components, or even to be tissue-specific [Charras, 2002].

In a cell, the cytoskeleton is a network of actin, tubulin, and intermediate filaments that modulates cell sensitivity to mechanical stimuli by adapting its structure to accommodate prolonged mechanical strains [Ko, 2000]. **It has been repeatedly demonstrated that one of the early responses to mechanical stimuli is an increase in intracellular free calcium concentration ($[Ca^{2+}]_i$)** [Hung, 1996] [Sharmaa, 1995]. In addition, some evidence suggests that cells experiencing mechanical forces may communicate their status to remote cells which are not under direct influence of these forces [Helmke, 2002].

Different methods such as dynamic loads [Rubin, 1984], homogeneous compression [Jones, 1991] and fluid flow [Hung, 1996], have been developed to apply a mechanical stimulus at the cellular level. However, only the AFM through **force spectroscopy** enables precise application of low forces to single cells, allowing with this quantitative measurement of single cell effects, cell elasticity [Radmacher, 1997], minimal disruption to cells [Haydon, 1996] and determination of cellular strain distributions during indentation [Charras, 2001].

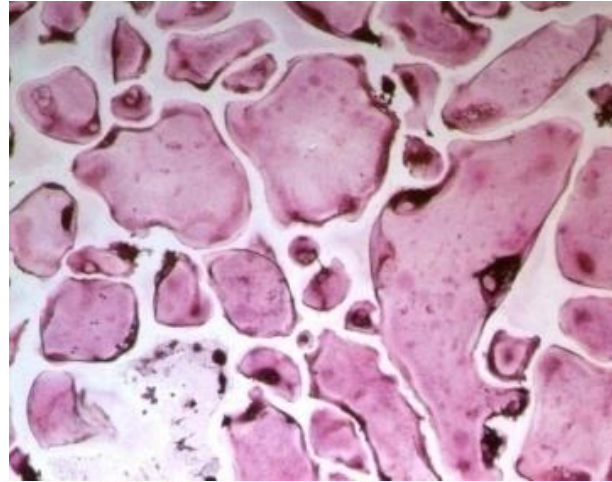
In this work, the magnitude of the mechanical strains to which cells respond was investigated using an AFM. Studies to confirm the chemistry of the signaling paths resulting from the strain imposition and inhibitors were investigated in another setup using pipette micro-injection.

4.1.2 Mechanical Stimulation of Cells

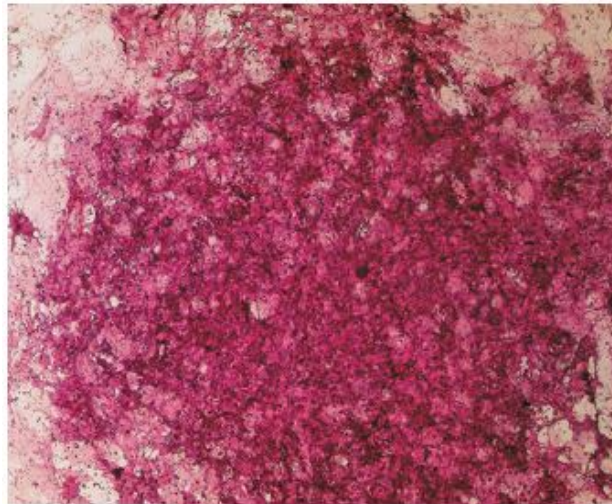
As mentioned above, this study was developed in an effort to determine, at the single cell level, the characteristic strains to which osteoblasts and

osteoclasts respond. To further understand the relationships between cell mechanics and mechano-sensitivity, in our experiments a co-culture of osteoclasts and osteoblasts from mouse bone marrow, and single cell type populations of osteoclasts formed from murine monocytic RAW 264.7 cells, and osteoblast-like cells formed from mouse mesenchymal C2C12 cells (see figure 4.2) were cultured.

A) RAW264.7 cells were cultured in the presence of RANKL for up to 8 days, and were used for experiments between day 4 and day 8. Illustrated are TRAP-positive multinucleated osteoclasts after 5 days of culture.



B) C2C12 cells were BMP transfected and cultured at density of 25000C/dish, in DMEM media +5ml PenStrep and 50ml FBS. Cells are differentiated at day 2-3. Illustrated is a monolayer of osteoblast-like cells obtained in these cultures. The illustrated cells were fixed at day 5 and stained for Alkaline Phosphatase.



C) *Bone Marrow* (primary cells) cells were cultured in the presence of RANKL and AA for up to 12 days, and were used for experiments between day 4 and day 12. Illustrated is bone marrow culture fixed at day 6 and stained for Alkaline Phosphatase (red) and TRAP (purple). Large TRAP-positive multinuclear osteoclasts are clearly visible within sheets of Alkaline Phosphatase-positive osteoblasts.

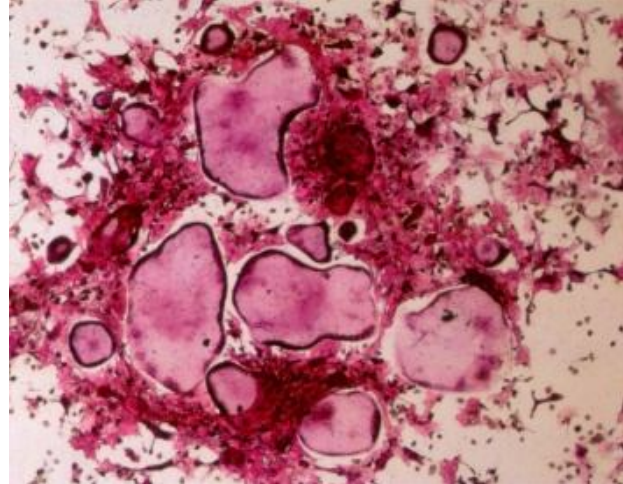


Figure. 4.2 Cultured Bone Cells. This figure illustrates the different types of cultured bone cells and the protocol followed to culture them for experiments.

In each experiment, a single cell was mechanically stimulated by gently indenting the tip of an AFM cantilever by making a F-D curve, the effects of varying the speed of indentation were ~~revised~~. The consequent changes in cytosolic free calcium concentration ($[Ca^{2+}]_i$) were recorded and analyzed.

The measurements were performed using a PPP-NCLAuD AFM probe from Nanosensors ($k=48N/m$ and $f=190kHz$). The tips were etched perpendicularly to the tip axis, using Focused Ion Beam (FIB). A tip diameter of $1\mu m$ was achieved as shown in figure 4.3. A ~~triggering~~ force of $2\mu N$ was applied during each indentation.

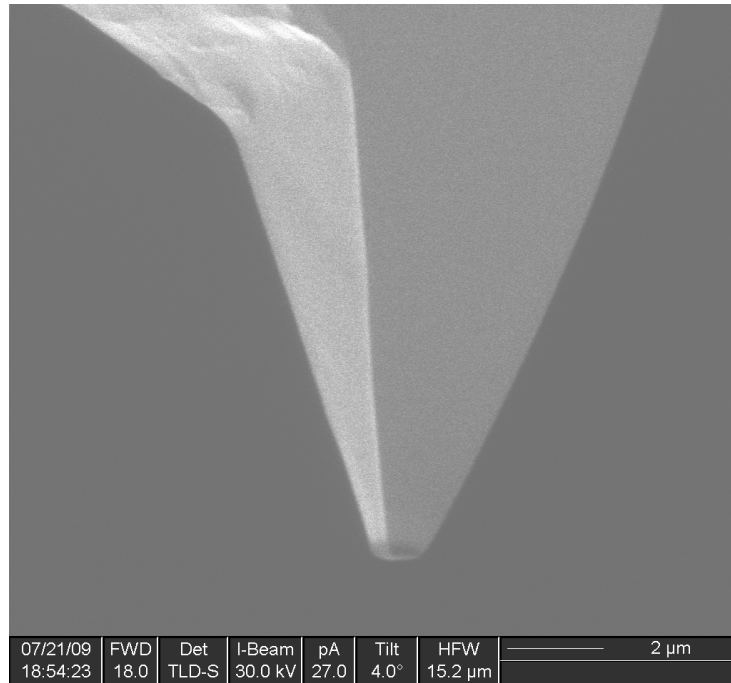


Figure. 4.3 NCLAuD cantilever tip etched through FIB. This image shows the tip end of the cantilever used on the force spectroscopy indentation experiments. The tip diameter was etched to 1 μm diameter

Despite their bluntness and high spring constant, these tips made possible to attain well defined contact areas and were able to resolve sub-cellular structures of living cells. These tips were used as well to induce Calcium signalling in response to mechanical stimulation as will be discussed in the following section.

4.1.3 Calcium Signaling in Bone Cells Induced by Mechanical Stimulation of a single Cell

Among the many methods of applying a mechanical stimulus onto a single cell, only atomic force microscopy (AFM) enables a precise application of very low forces. The mechanical stimulation and signaling induced [Leidert, 2006] will be described in the following sections.

4.1.3.1 Calcium Signaling in Bone Cells

The fact that one of the early responses to mechanical stimuli is an intracellular increase in the free Calcium concentration [Hung, 1996] will allow us to test the cytosolic free calcium ($[Ca^{2+}]_i$) concentration by fluorescently labeling it.

To examine the effect of the mechanical stimulation in our experiments, cultured cells were incubated in medium for 30 min with 1.5 μ l Fluo4-AM dye from Invitrogen, which fluorescence can be strongly excited at 488 nm using an Argon-Ion laser (see Appendix C for details). After loading the dye, the dish was incubated at 37°C in light tight conditions. Then, the medium with the dye was aspirated and cells were washed with 1 ml physiological buffer (130 mM NaCl, 4 mM KCl, 10 mM glucose, 1 mM MgCl₂, 1 mM CaCl₂, HEPES 20 mM). The dish was then put on the Open Fluid cell and 1 ml/medium was added. The holder was heated up to 37°C for and during the experiment.

Intracellular calcium levels in response to the mechanical stimulation were assessed via the inverted optical microscope through a high NA Oil Objective (Olympus PLAPON 60X). Movies were acquired using the 512F Cascade Camera using Image-Pro software capturing frames at intervals of 250ms in movies of 200 frames, i.e. 50s total. The fluorescence temporal evolution was recorded in the same field of view (300 μ m in length). ImageJ software was then used to stack a profile of the intensity in time, at several locations within and between cells.

A single osteoclast and osteoblast was mechanically stimulated, and $[Ca^{2+}]_i$ changes were recorded and an intensity profile was stacked as in figure 4.4 (to watch the movie double click on the image in figure, only works for word documents, otherwise please refer to Appendix D for a sequence of the movie). The $[Ca^{2+}]_i$ concentration during the first seconds before stimulation of the cell are referred to as the basal $[Ca^{2+}]_i$ level. In response to the stimulation, the cells exhibited a rapid increase in $[Ca^{2+}]_i$ level, which declined back to around the basal level after a few seconds of providing the stimulation. The $[Ca^{2+}]_i$ transient of the stimulated cell will be from now on called the primary response.

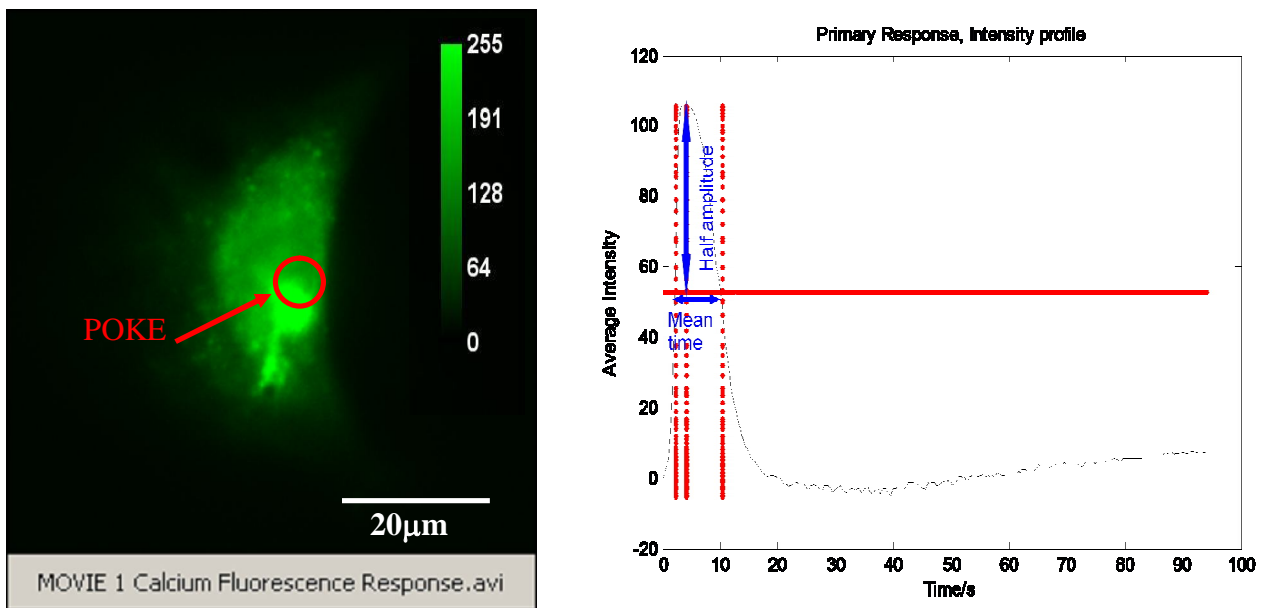


Figure 4.4 Bone Cell response to mechanical stimulation. On the left, a movie presenting the increase in mean fluorescence intensity after a F-D curve was done to mechanically stimulate it. On the right, a graph showing the fluorescence intensity after mechanical stimulation was applied (at $t=0s$). The intensity level sharply increases and decays after few seconds from the stimulation moment. Only a small amount of cellular material was displaced by indentation as can be verified from [in](#) movie.

A single $[Ca^{2+}]_i$ transient elevation was noted in each of the indentation experiments. To further analyze the responses from stimulated cells a program in matlab was created. The **half Amplitude** $[(\max [Ca^{2+}]_i - \text{basal } [Ca^{2+}]_i)/2]$, **mean time** of response, and an estimate of the relative amount of

$[Ca^{2+}]_i$ [Amplitude*mean time] were determined for each stimulated cell at different speeds (Fig. 4.4).

Throughout the analysis of non-stimulated cells movies, dye bleaching was sometimes observed, although the pattern suggested an exponential decay, no approximations to account for bleaching were intended and raw data was used for analysis. All types of cells exhibited $[Ca^{2+}]_i$ transient elevation.

The frequency of responses to mechanical stimulation, both in osteoclasts and osteoblasts, were examined. The following figure (4.5) shows an estimate of the percentage of primary responders as function of the indentation speed and cell type.

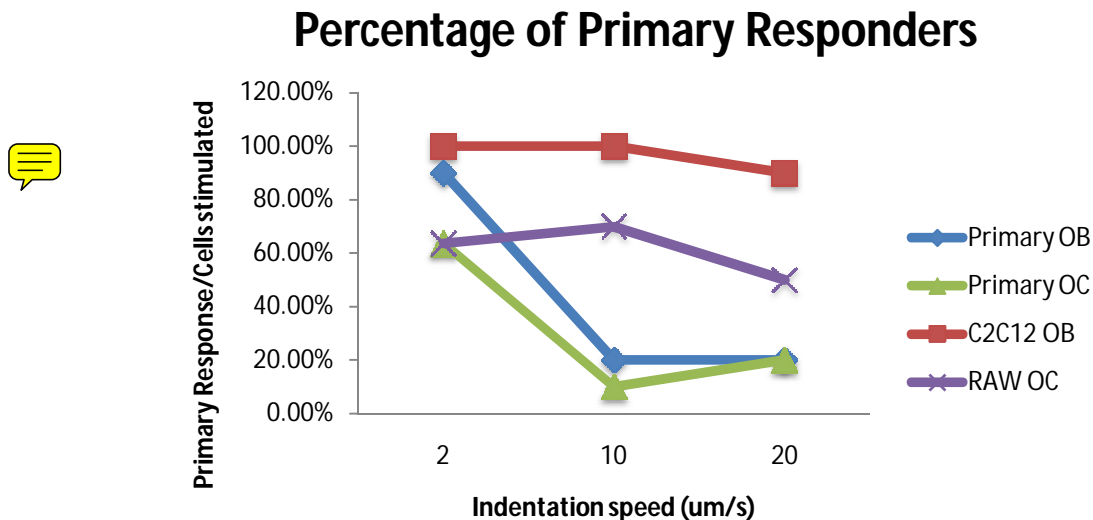


Figure 4.5 Frequency of Primary responses. This graph presents the percentage of primary responding cells as a function of the indentation speed. 10 cells were tested of each type of cell and each speed.

A significantly higher amount of cells responded among the ones which were mechanically stimulated at lower speeds. Moreover, primary cells, both from the same cell culture, in the same dish, were randomly indented and they appear to display a similar behavior demonstrating a large drop in percentage of responders from $2\mu\text{m/s}$ to $10\mu\text{m/s}$ (with 90% of primary osteoblasts responding at $2\mu\text{m/s}$ drops and only 20% at $10\mu\text{m/s}$, similarly

63.6% of primary osteoclasts responded at 2 μ m/s , while only the 10% at 10 μ m/s).

In addition to generating $[Ca^{2+}]_i$ transient changes in stimulated cell, mechanical stimulation induced delayed transient $[Ca^{2+}]_i$ elevations in neighbouring non-connected cells, or secondary responders, which, in our setup were only obvious for osteoblasts. No secondary responders were observed in osteoclasts, however, from experiments with pipette microinjection, the appearance of primary and secondary responses was confirmed in both osteoblasts and osteoclasts.

The following figure (4.6) shows the percentage of secondary responses as a function of the indentation speed.

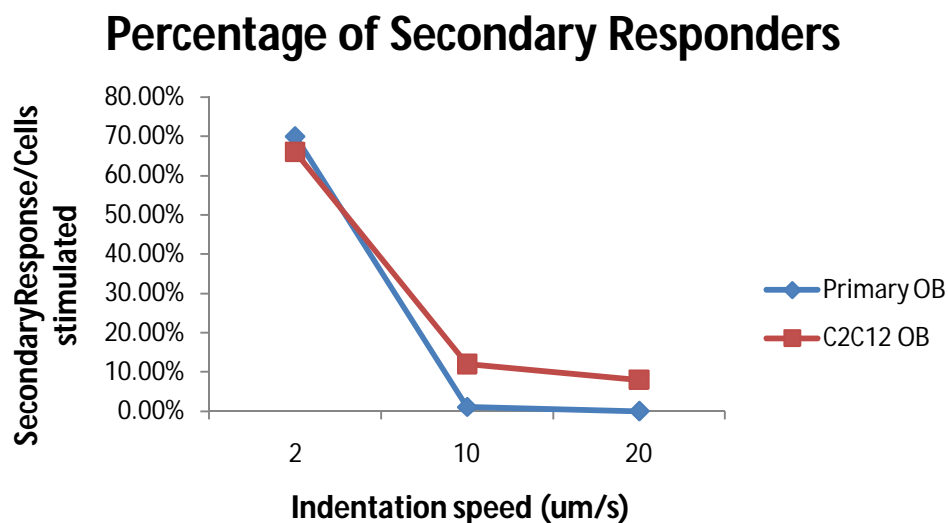


Figure 4.6 Frequency of Secondary responses. This graph presents the percentage of secondary responding cells over stimulated cells as a function of the indentation speed. 10 cells of each type were tested for each speed.

It was noted that secondary responders manifested only when there was a primary responder. The graph above shows the number of secondary responding cells with respect to the cells stimulated, as a function of speed; this includes the probability of a cell to respond, and its probability to induce a secondary response.

Within osteoblasts, a significantly higher amount of secondary responders was observed among the cells stimulated at low speed with respect to the ones stimulated at 10 and 20 $\mu\text{m/s}$. In 30% of the experiments at low indentation speed (2 $\mu\text{m/s}$), more than a single cell presented a secondary response. Osteoblasts exhibited, as before, a large difference in percentage of responders from 2 $\mu\text{m/s}$ to 10 $\mu\text{m/s}$ compared to the difference from 10 $\mu\text{m/s}$ to 20 $\mu\text{m/s}$. No secondaries were observed in Primary osteoblasts at 20 $\mu\text{m/s}$.

Since the probability of a cell to respond as a primary is included in the calculation, primary cells were likely to have lower number of secondaries than C2C12 cells and to drop significantly when varying from 2 to 10 $\mu\text{m/s}$. However, in average, every time an osteoblast was stimulated, it induced the same number of secondary responders around it.

By analyzing transients in secondary responders it was noticed that the pattern was different from the one in primary responders. In the primary responders, $[\text{Ca}^{2+}]_i$ transients had always a single peak, $[\text{Ca}^{2+}]_i$ transients in secondary responders exhibited two different patterns, either one peak or oscillatory pattern were observed (Fig, 4.7).

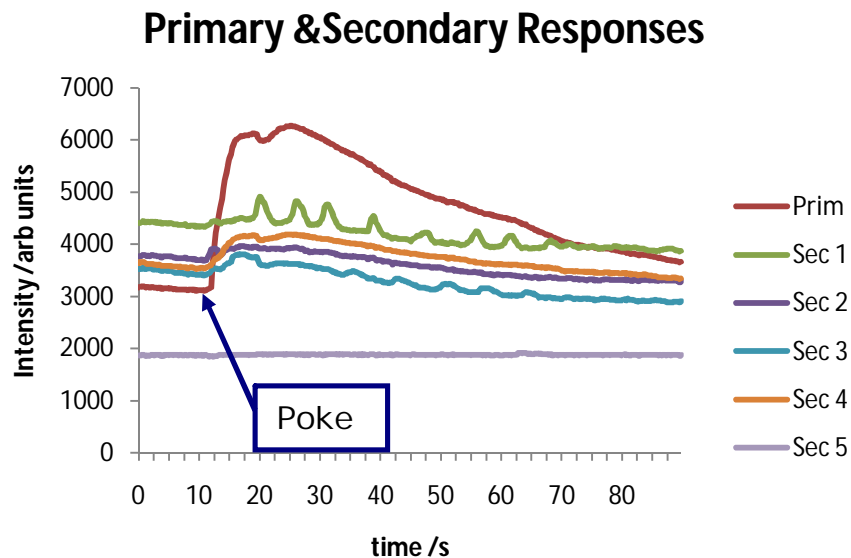


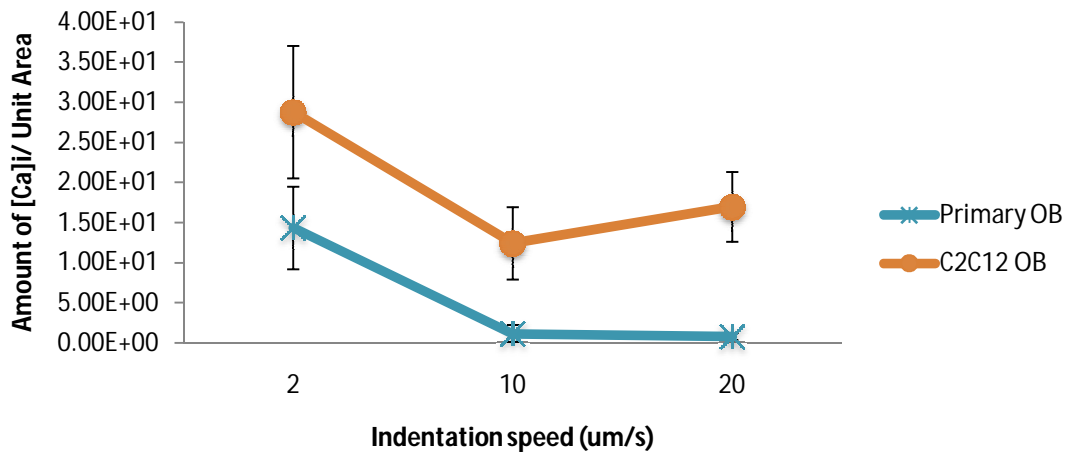
Figure 4.7 Primary and Secondary responses. The intensity profile of different cells within the same field of view is presented in this graph. Labeled in red "Prim", the primary response. Other, non-connected, cells present an increase in mean fluorescence intensity i.e. in the intracellular, $[\text{Ca}^{2+}]_i$ level, after stimulation. Mechanical stimulation was applied (at t=10s). This experiment was done in C2C12 cells. A triggering force of 2 μN was selected.

Aware of the fact that secondary responses don't exhibit the same pattern as primary responses they have been analyzed with a different intention since their amplitude and duration are not always the same. Given that secondary responses appear in non-connected cells in the surroundings of the primary, through data analysis it has been found that the amplitude of response to the mediator decreases with distance and the apparent diffusion coefficient increases with distance. It is likely to suggest there is a soluble mediator being released by the primary cell, which diffuses through the media. Inhibitor studies suggest this mediator is likely associated to ATP as suggested by [Leidert, 2006], ADP or some other degradation product, acting through suramin-sensitive P2 receptor (these studies have been done in the pipette microinjection setup and won't be further discussed here). Understanding calcium cell signaling may help to elucidate the biophysical transduction mechanism(s) mediating the conversion of mechanical deformation or injury to a cellular signal, this work becomes a possible extension of this project.

Evidence has been provided to support the fact that $[Ca^{2+}]_i$ oscillations increase both the efficacy and the information content of $[Ca^{2+}]$ signals that lead to gene expression and cell differentiation [Dolmetsch, 1998]. Other experiments by [Charras, 2002] suggest that the secondary responses in bone cells arise in response to the strain generated in the micro-tubular and the vimentin net-works in the cell, they suggest other cells communicate to the primary cell through these networks and the signal is exchanged through them. On the other hand, in our experiments the cells are not necessarily connected.

Provided that all cell types exhibited primary responses, we can analyze how the amount of $[Ca^{2+}]_i$ in the response varies with the indentation speed for each cell type (Fig. 4.8).

Amount of Ca over Area OB



Amount of Ca over Area OC

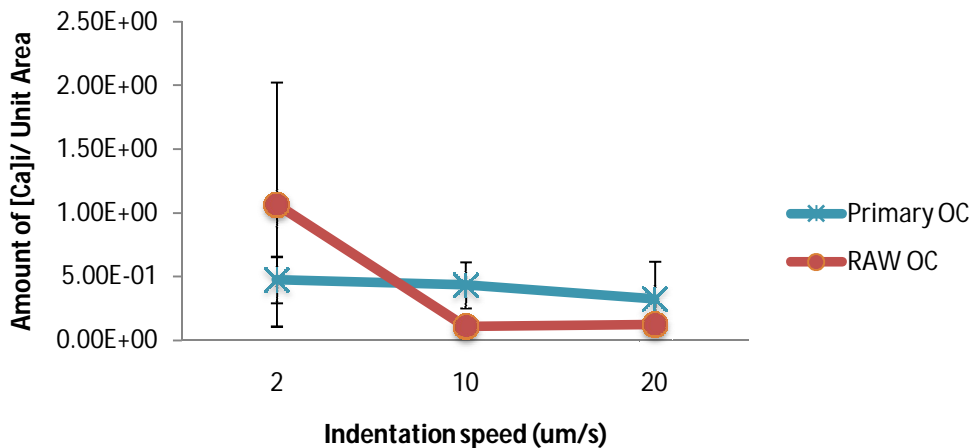


Figure 4.8 $[Ca^{2+}]_i$ Amount per Unit Area in Primary responses. These graphs represent the “volumetric amount of $[Ca^{2+}]_i$ ” in primary responders as function of the indentation speed. 10 cells of each type were tested for each speed.

To account for the fact that osteoclasts are much bigger in volume than osteoblasts, a “Volumetric $[Ca^{2+}]_i$ Amount” or “ $[Ca^{2+}]_i$ density” in each response was estimated by normalizing the amount of $[Ca^{2+}]_i$ to the 2D area of the cell in the movies, as an approximation of their size. Overall, the $[Ca^{2+}]_i$ density in the responses is significantly higher in osteoblasts,

compared to osteoclasts. In addition, the basal levels of $[Ca^{2+}]_i$ were in fact, significantly higher in osteoblasts, compared to osteoclasts.

In order to summarize the results in this section so far, we can point out that the $[Ca^{2+}]_i$ response frequency varied depending on the speed of the mechanical stimuli, so there is likely a time required to detect the deformation. As a result to the initial $[Ca^{2+}]_i$ transient in the stimulated cell, there is a signal being communicated to other neighboring, non-connected cells which is likely ATP diffusing through the media.

4.1.3.2 Force spectroscopy

To characterize the mechanical stimulation required to induce a detectable $[Ca^{2+}]_i$ response and better understand the changes in intracellular calcium reactions and signaling, the AFM was used to modulate the applied force and measure the deformation induced at the single cell level.

Mechanical stimulation was provided by performing a FD curve on top of the cell at different speeds. Blunt tips described in section 4.1.2 enabled to attain well defined contact areas causing minimal disruption. The analysis of features such as cell deformation, membrane rupture force and penetration were performed after indenting the surface of the cell with the cantilever tip (see fig. 4.9). In addition, the measurements allowed determination of the apparent elasticity of the cell.

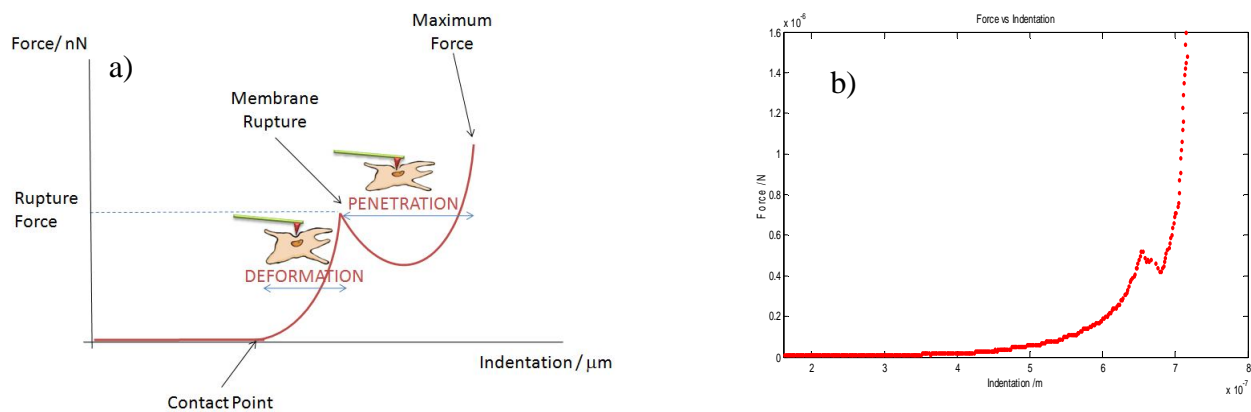


Figure. 4.9 Approach F-D curve on a cell showing membrane rupture. Figure a) represent the FD curve taken on a cell exhibiting cellular membrane rupture, the deformation, penetration and membrane rupture force are common features seen in cell indentation experiments. After the contact point the cantilever deforms the cell until it reaches the force required to rupture the membrane of the cell. After membrane rupture, the cantilever penetrates the cell while compressing some of the cellular organelles until the trigger point is reached. Figure b) is the approach part of a FD curve taken over a C2C12 cell.

It is to be mentioned that no sign of adhesion between indenter and cell was noticed in the AFM retraction curves. The elastic modulus of the cells was estimated from fitting the spherical indenter Hertz model. This assumption

was proposed by [Radmacher, 1993] for a blunt pyramidal tip, however, this model fails for indentations larger than the apparent radius of curvature of the tip. For wider indentations, a blunted cone model has been developed by [Rico, 2005].

The Young modulus (elastic modulus) was calculated from each of the indentation curves in all the experiments using the Hertzian spherical indenter model. The elastic modulus obeys a power law behavior following eq. 1.6:

$$Fc = \frac{4ER^{1/2}}{3(1-\nu^2)} \delta^{3/2} \quad (\text{Eq. 1.6}).$$

Taking the logarithm of this equation:

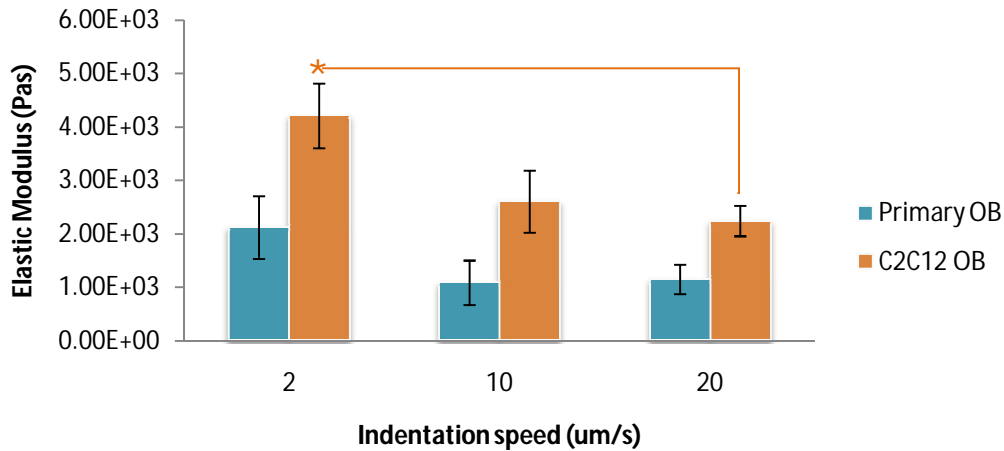
$$\log(Fc) = \log\left(\frac{4ER^{1/2}}{3(1-\nu^2)}\right) + \frac{2}{3}\log(\delta)$$

$$\log(Fc) = \log(E) + \alpha + \frac{2}{3}\log(\delta)$$

where α is a geometrical constant. A linear fit with slope of $2/3$ was made to the $\log(\text{Force})$ vs. $\log(\delta)$ plot. α Was then subtracted to the vertical intersection (the $\log(F)$ axis) and E was calculated from the resulting constant $\log(E)$, the Young's modulus was found for each of the experiments. The contact point of the probe with the cell was determined by estimating where the linear behavior (non-contact region) of the force curve, became a quadratic function (contact region). A maximum force of 5nN was taken as the superior force limit for the elastic modulus calculation. The number of points in the vicinity of the interval selected was slightly varied in order to get the best fit.

The following figure (4.10) shows the Elastic modulus estimate for each type of cell at different rates.

Elastic Modulus OB



Elastic Modulus OC

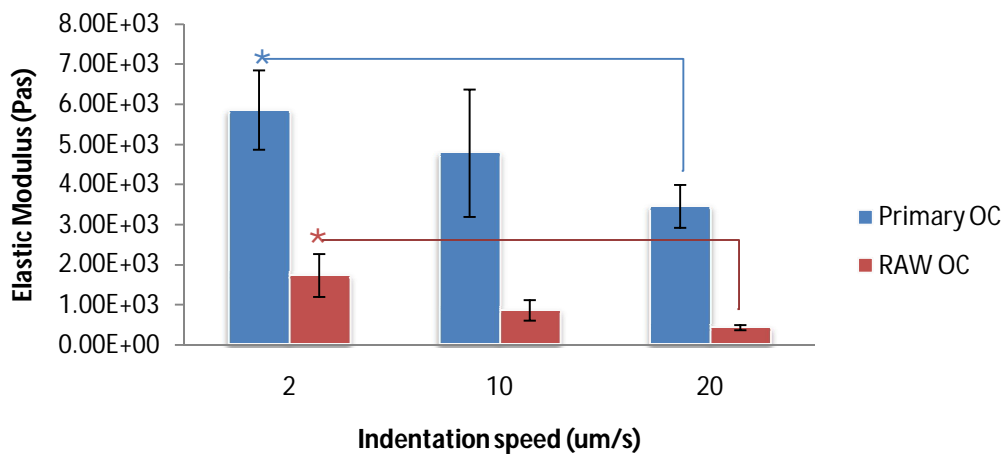


Figure. 4.10 Elastic Modulus in different Bone Cells. These graphs illustrate the Young's Modulus of each cell population used during experiments. The calculations were estimated from the indentation curves used to provide mechanical stimulation to the cells. Osteoblasts, at the top, and osteoclasts at the bottom. 10 cells from each type were stimulated at each of the speeds.

Analysis suggests that there is an inverse relationship between the Young's Modulus and the speed of indentation. Therefore, while the speed increases, the apparent Young's modulus decreases for all types of cells. It is to be mentioned that the tip shape, area and deformation induced in the cells is large, and the forces applied are big compared to usual forces applied to estimate this modulus [Li, 2008] (this will be discussed in the further detail) compared to previous studies [Takai, 2005], therefore the measured

elastic modulus is likely to represent an apparent modulus influenced by the cell membrane and other less superficial structures inside the cell rather than only a superficial property in an inelastic regime of the material [Hassan, 1998], [Costa, 1999].

The following table is provided to compare the effects of each parameter in the FD curve and investigate how they produce a detectable $[Ca^{2+}]_i$ response. Knowing that the largest amount of responses happen at low speeds of indentation, the experiments at low $2\mu\text{m/s}$ and fast speed $20\mu\text{m/s}$ will be compared. The following tables show the average values obtained for each of the cell populations.

		Osteoblasts			
		Primary OB		C2C12 OB	
	Speed	$2\mu\text{m/s}$	$20\mu\text{m/s}$	$2\mu\text{m/s}$	$20\mu\text{m/s}$
Puncture force	(μN)	0.21 ± 0.04	0.41 ± 0.11	0.26 ± 0.05	0.43 ± 0.07
Deformation	(μm)	1.14* ± 0.14	1.31* ± 0.25	0.64* ± 0.08	0.86* ± 0.14
Penetration	(μm)	0.09 ± 0.01	0.10 ± 0.03	0.08 ± 0.01	0.08 ± 0.01
Elastic Modulus	(KPas)	2.12 ± 0.58	1.15 ± 0.27	4.21* ± 0.60	2.24* ± 0.28

		Osteoclasts			
		Primary OC		RAW OC	
	Speed	$2\mu\text{m/s}$	$20\mu\text{m/s}$	$2\mu\text{m/s}$	$20\mu\text{m/s}$
Puncture force	(μN)	0.25 ± 0.06	0.14 ± 0.04	0.17 ± 0.03	0.31 ± 0.08
Deformation	(μm)	1.52* ± 0.17	2.44* ± 0.43	2.22* ± 0.48	5.46* ± 0.72
Penetration	(μm)	0.09* ± 0.01	0.23* ± 0.04	0.39 ± 0.17	0.27 ± 0.03
Elastic Modulus	(KPas)	5.86* ± 0.98	3.46* ± 0.53	1.73* ± 0.53	0.43* ± 0.06

Table 4.1 FD curve features for different cell types.

From the average results in the table for **osteoblasts** (at the top), in different cell populations, the puncture force increases with the speed. It has been previously suggested that the penetration force increased with the speed of penetration, given that at high enough tip velocities rupturing the membrane while progressively compressing a cell can be avoided [Hategan, 2003]. However the sampling distribution is not significantly different among each speed according to the TTEST.

The deformation induced in the cell before the puncture force is significantly different for different speeds of indentation, meaning that the deformation increases with higher speed of indentation. Accordingly, when higher deformation is induced, the elastic modulus decreases, as expected from softer materials. Additionally, the deformation induced in Primary osteoblasts and C2C12 at speed of $2\mu\text{m/s}$ is significantly different among cell populations. This variation is expected, since C2C12 cells are used as for modeling Primary OB.

From the results in the table for **osteoclasts**, in the different cell populations, the puncture force seems to exhibit no correlation between the low speed ($2\mu\text{m/s}$) indentation compared to the $20\mu\text{m/s}$ indentation, suggesting this is due to their large variations in volume and the lack of enough samples for statistics. However, the deformation induced before membrane rupture is significantly higher at higher speeds of indentation, as happens for osteoblasts. In addition, we confirm the elastic modulus decreases with higher deformation as expected.

There are no significant changes in penetration. This is to be confirmed with additional experiments which are expected to improve the statistics. So far, it seems the penetration is independent on the speed of indentation.

In all the cases, the deformation increases with higher speed of indentation, accordingly, when higher deformation is induced, the elastic modulus decreases, therefore, the cell appears to be softer at higher speeds. Variations in the viscoelastic behavior of the cell were expected, and apparently, for this tip geometry, **at low indentation speeds**, the following happens:

- There is less membrane deformation, => more horizontal displacement

- More time to detect/adjust to the deformation

Suggesting that the $[Ca^{2+}]_i$ responses are not associated with net membrane deformation, but rather with the time to detect and adjust to it. The following figure (4.11) may help to understand the observations.

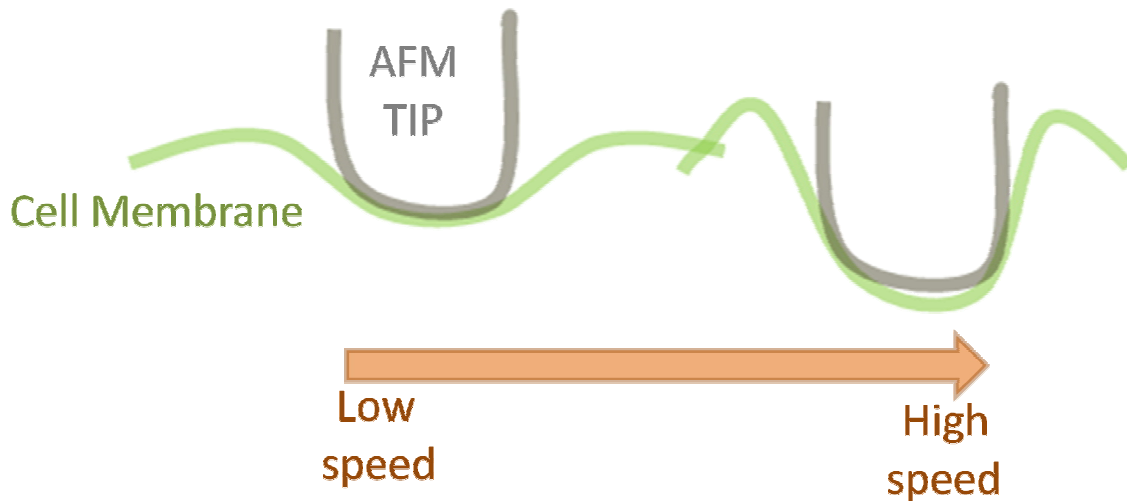


Figure. 4.11 Membrane Deformation with speed. This image represents the effect of increasing the indentation speed on the membrane deformation induced.

It is now worth to remember that more secondary responses appear also at lower indentation speeds and, in our setup, they appear only in osteoblasts. Taking into account the fact that there is no significant difference in penetration, the following is suggested:

- Given that **osteoclasts exhibit only primary** $[Ca^{2+}]_i$ responses, secondary responses may be triggered by an injury that is large relative to the cell size. Since OB are smaller, critical injury will be reached with a smaller hole size.

Only for the sake of comparison, if we look into Primary cultures, we will find the following:

Osteoblastic cells size $\approx 3000 \mu\text{m}^3$

Osteoclast cells size $\approx 300000 \mu\text{m}^3$

Actual hole size $\approx 1 \mu\text{m}^2$

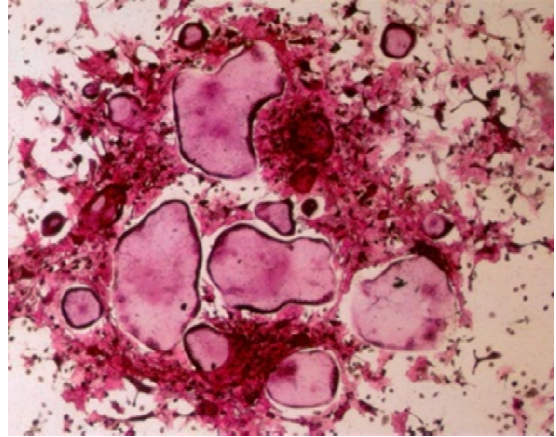


Figure. 4.12 Size of osteoblasts and osteoclasts in primary cells. This image illustrates the difference in volume among osteoblasts and osteoclasts.

Osteoclasts are more than one hundred times bigger than osteoblasts, the relative hole size and/or sufficient stimulus detection time is likely important for triggering a $[\text{Ca}^{2+}]_i$ response. However, the basal $[\text{Ca}^{2+}]_i$ in osteoclasts is significantly lower compared to osteoclasts.

As for the secondaries, propagation of mechanical stimulation to secondary cells likely requires a critical size defect in the primary cell.

4.2 Conclusions

Modeling the mechanical stimulation at the single cell level allowed us to study the mechano-transduction process and to elucidate some of the signaling pathways through which a single stimulated cell can produce and induce calcium signaling.

The presence of primary responses confirmed in response to mechanical stimulation. Secondaries were only induced when there was a primary responder.

The speed of indentation has an effect in the cell responsiveness, the percentage of responders. A significantly higher amount of cells responded among the ones which were mechanically stimulated at lower speeds. This

suggests that there is likely a time required to detect the deformation in order to produce a detectable response.

As a result to the initial $[Ca^{2+}]_i$ transient in the stimulated cell, there is a signal being communicated to other neighboring, non-connected cells which induces secondary responses. It is likely to suggest there is a soluble mediator being released by the primary cell, which diffuses through the media. Inhibitor studies suggest this mediator is likely associated to ATP as suggested by [Leidert, 2006], ADP or some other degradation product, acting through suramin-sensitive P2 receptor.

Basal $[Ca^{2+}]_i$ level is higher for osteoblasts and a significantly higher amount of secondary responders was observed among the cells stimulated at low speed.

Analysis of the average of the results for each rate within each cell population suggests that there is an inverse relationship between the speed of indentation and the cell Young's Modulus, suggesting that the measured elastic modulus is likely to represent an apparent modulus influenced by the cell membrane and other less superficial structures inside the cell.

The deformation increases with higher speed of indentation, accordingly, when higher deformation is induced, the elastic modulus decreases, therefore, the cell appears to be softer at higher speeds. This suggests that there is less membrane deformation, but more horizontal displacement and more time to detect/adjust to deformation. Suggesting that the $[Ca^{2+}]_i$ responses are not associated with net vertical membrane deformation only, but rather with the time to detect and adjust to it.

Given the fact that osteoclasts are more than one hundred times bigger than osteoblasts, the relative hole size and sufficient detection time is likely important for triggering a $[Ca^{2+}]_i$ response. Propagation of secondary responses likely requires a critical size defect in the primary cell, which was not reached for osteoclasts during the experiments.

Studies in the calcium cell signaling and the force spectroscopy have elucidated the some of the biophysical transduction mechanism(s) mediating the mechanic stimulation and its conversion to a cellular signal.

General Conclusions and Outlook


Along this thesis the implementation and development of tools applied for the study of cells in physiological environments have been described and characterized, localized illumination towards SNOM, fluorescence and AFM force spectroscopy in biological samples under liquid environments techniques and tools were combined. Such tools have proved to work in solutions with very low applied forces and increased resolution and sensitivity in opposition to the damping and noise induced in liquid environments [Fukuma, 2005].

1. Dynamic atomic force microscopy using frequency modulation (FM) mode was successfully extended to liquid environments, and has enabled measurement and determination of ordered liquid layers above mica.
2. Stable imaging and force spectroscopy was demonstrated in liquid using a "diving bell" array using home fabricated bent fiber probes based on SNOM cantilevers [LeDue, 2008].
3. AFM spectroscopy and fluorescence techniques were successfully combined and helped provide some insight on the mecano-transduction mechanisms in living cells.

This work was done under tutoring of Jeff LeDue, who provided me with the knowledge and specifications to work with these tools and then commissioned me to extend the microscope's capabilities; results 1 and 2, corresponding to chapters 2 and 3 are attributed entirely to his work.

Future work involves combining AFM force spectroscopy and dynamic FM-AFM mode biological samples under liquids using the “diving bell” to study their mechanical properties and the hydration structures ionic active regions. Localized fluorescently targeted regions ~~can be provided with local illumination~~ using SNOM based tips to minimize the effect of the light-dependent breakdown of the chromophores, which generate reactive oxygen species contributing to bleaching and damage in the cell tissues [Pervaiz, 2006].

~~The following gathers~~ the conclusions and possible extensions of each section of the thesis:



In chapter 2: Dynamic atomic force microscopy using frequency modulation (FM) mode was successfully extended to liquid environments, and has enabled measurement and determination of ordered liquid layers above mica. It has been shown that for an AFM mounted on an inverted optical microscope, with the sample in a fluid cell, the contribution to the noise density due to vibrations is significant and can dominate over noise from the deflection sensor for deflection sensor noise densities $< 200 \text{ fm}/\sqrt{\text{Hz}}$. Modeling has shown that despite the presence of the noise from all sources, including vibrations, the spacing of the hydration peaks can be reliably recovered by fitting an empirical force law given that around the minima and maxima the gradient of the frequency shift is ~ 0 , which means the contribution from vibrations is reduced. The measurement of the hydration structure on the MFP-3D-BIO in water and OMCTS above mica has been demonstrated. Average peak spacing of 0.24 nm for water and 0.75 nm for OMCTS were recovered. ~~Additionally when comparing~~ FM and AM hydration measurements using Nanosensor PPP-FMAuD tips. The hydration peaks ~~have been~~ found to be readily observable using the AM method. Further study is needed to determine if there is an intrinsic advantage to the AM measurement in liquid as practically it simplifies the experimental setup: with the addition of a band-pass filter and an amplifier these types of measurements can be made on a commercial “bio-AFM” out-of-the-box.

The future aim of this study points towards ~~the study of~~ the role of water and ions in ~~genetically labeled~~ regions in the cell surface targeted for hydration structure measurements in vivo through combined optical and atomic force microscopy. Application of these techniques can lead to a better understanding of the distribution of molecules and ligands around

the cells and their role in the kinetic characteristics of the interaction with the membrane receptors (ligand-receptor interactions) [Vauquelin, 2009].

In chapter 3: Stable imaging and force spectroscopy ~~has been~~ demonstrated in liquid using a “diving bell” array using home fabricated bent fiber probes [LeDue, 2008]. The fabrication process of the tips used, based on Scanning Near-field Optical Microscopy, ~~has been detailed~~. It ~~has been~~ shown the “diving-bell” allows operation in liquid while maintaining a high Q factor. Not only does this allow stable imaging using NC-AFM feedback, but also ensures that, even with mechanical excitation of the cantilever's motion, the cantilever is driven at resonance and not some other ~~fake~~ peak caused by the combined motion of the cantilever plus its holder and the high drive required to ~~reach the oscillation set point~~, as commonly happens for liquid environments. Single resonance peak in the cantilever ~~tune~~ allows the force to be calculated from the frequency shift, permitting quantitative force spectroscopy in a liquid environment. Imaging forces can be maintained within reasonable limits for soft biological samples and live cells, and the potential exists for both high resolution topographic and optical imaging. The ability to combine quantitative force spectroscopy with local fluorescence microscopy makes using bent fiber probes with NC-AFM a promising technique for studies of bio-molecules and live cells in physiological solution.

In chapter 4: AFM spectroscopy and fluorescence techniques were successfully combined and helped provide insight on the mecano-transduction mechanisms in single bone cells. $[Ca^{2+}]_i$ Signaling pathways were ~~induced on the cells~~ through mechanical stimulation. The presence of primary responses was confirmed in response to mechanical stimulation, suggesting the initial $[Ca^{2+}]_i$ transient in the primary cell was induced by cell deformation and injury, and the signal was communicated ~~a signal~~ to other neighboring, non-connected cells, inducing secondary responses. Secondary responders were only induced when there was a primary responder suggesting the release of a soluble mediator through the injury (likely ATP, as suggested by [Leidert, 2006], ADP or some other degradation product, acting through suramin-sensitive P2 receptor) which diffuses through the media and induces a response on the surrounding cells.

The deformation increases with higher speed of indentation, ~~accordingly,~~ when higher deformation is induced, the elastic modulus ~~decreases,~~ therefore, the cell appears to be softer at higher speed of indentation. When

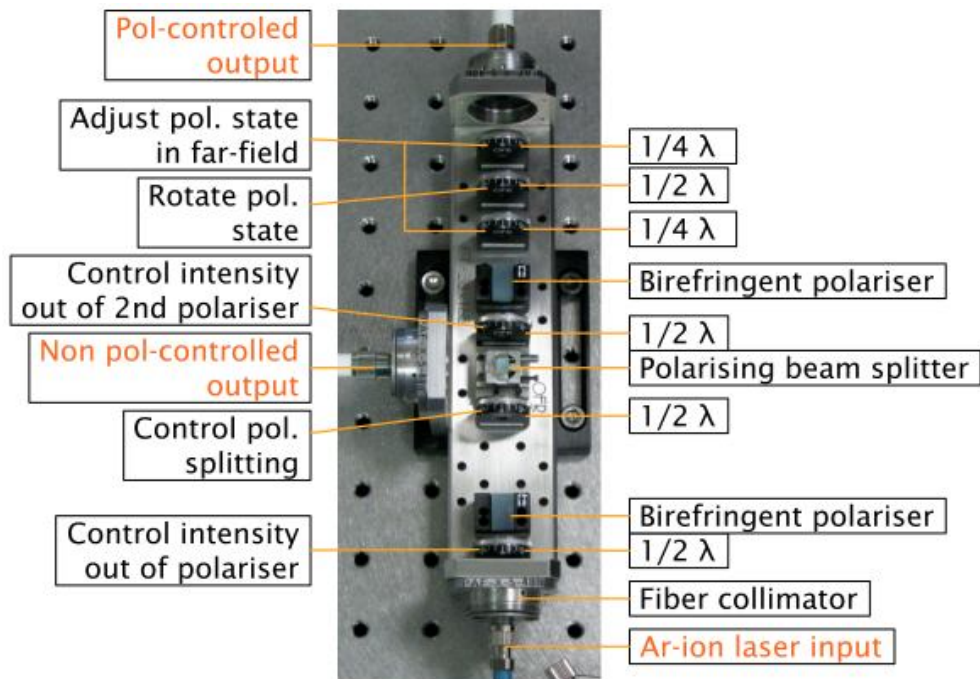
higher deformation is induced a lower amount of energy is ~~suggested to be required to deform the membrane, taking into account that the cell has less time to detect and adjust to the deformation imposed.~~ Accordingly, when indentations at low speed are imposed, the cell appears to be stiffer suggesting there is less membrane deformation but more horizontal displacement and, consequently, more time to detect/adjust to deformation. In this case more energy is put into the cell to induce vertical deformation. Recent experiments suggest that deformation of the cell induces local $[Ca^{2+}]_i$ elevations around the poke region. There has been no confirmation of the existence of secondary responders. Further experiments are required to confirm that there is a larger region of the cell around the poke where a $[Ca^{2+}]_i$ transient is induced.

The $[Ca^{2+}]_i$ responses are not associated with net membrane deformation, but rather with the time to detect and adjust to it. The speed of indentation has an effect in the cell responsiveness, a significantly higher amount of cells responded among the ones which were mechanically stimulated at lower speeds, suggesting that there is likely a time required to detect the deformation in order to produce a detectable response. Basal $[Ca^{2+}]_i$ level is higher for osteoblasts and a significantly higher amount of secondary responders was observed among the osteoblasts stimulated at low speed compared to osteoclasts, suggesting that there is more concentration of the mediator in osteoblasts compared to osteoclasts even though they exceed osteoblasts more than one hundred times in volume. It was noticed that the amount $[Ca^{2+}]_i$ in the response does not depend on the indentation speed within the same population and we suggest the relative hole size and sufficient detection time is likely important for triggering a $[Ca^{2+}]_i$ primary response. The signal propagation to secondary responders likely requires a critical size defect in the primary cell, which was not reached in our experiments for osteoclasts. Modifications in time resolution both of the sequence and the force curve are required to enable precise determination of the essential requirements to induce a global $[Ca^{2+}]_i$ elevation. As well, a greater number of experiments is necessary to reinforce and clarify some of the statements above mentioned.

Appendix A. Laser beam splitter adapted Scanning Near-field Optical Microscopy.

The Laser source is composed by an Ar-ion laser from Melles Griot (43 Series Ion Laser) on an OFR FiberBench with polarizers and waveplates


The laser source is an air-cooled Ar-ion laser with lines selectable from 457 to 514 nm. Its beam is injected into a fiber optics bench with 1/2 and 1/4 wave plates and polarizer filters, allowing with this to control the intensity and the polarization state of the output. A polarizing beam splitter separates the beam into two outputs with and without polarization control:



Appendix B. Phase contrast setup.

For alignment of the Asylum phase contrast illuminator, here's a rough outline of the steps:

First center and focus the sample plane, using the controls on the head:

1. Bring the AFM tip within 0.5 mm of the surface. Center the AFM tip on the optical field of view. Select the 10x/Ph1 objective lens if possible.
2. Focus on the AFM tip.
-  3. Close the field diaphragm (lever on the side of the tube).
4. Using the knobs on the back of the head, center the field diaphragm on the AFM tip.
5. Using the brass ring on the back of the head, focus the field diaphragm in the same plane as the AFM tip. It will be blurry at high magnification just make it as sharp as possible.
6. Open the field diaphragm.

Then center and focus the phase ring, using the controls on the pillar:

1. Put the Bertrand lens or centering telescope in place.
2. Focus the Bertrand on the dark ring in the objective lens.
3. Using the Z knob on the pillar, focus the edge of the bright ring to be in the same plane as the dark ring.
4. Using the XY knobs on the pillar, center the bright ring on the dark ring. For Ph2, adjust the XY to maximize the width of the bright crescent and ensure that it is fully enclosed within the dark ring.
5. Remove the Bertrand and proceed with imaging.

You may need to make minor readjustments if you change the field of view or the tilt of the head. Usually it suffices to tweak the XY knobs on the pillar.

Appendix C. Absorption and Emission Spectra Fluo-4.

Fluo-4 dye exhibited high fluorescence emission, a high rate of cell permeation, and a large dynamic range for reporting $[Ca^{2+}]$ around a $K_d(Ca^{2+})$ of 345 nM as reported by [Gee, 2000]. Because of its higher fluorescence emission intensity, fluo-4 can be used at lower intracellular concentrations, making its use a less invasive practice.

Several Ca^{2+} -indicators related to fluo-4 having lower affinities for Ca^{2+} that are useful in cellular studies requiring quantification of higher $[Ca^{2+}]$ have also been developed.

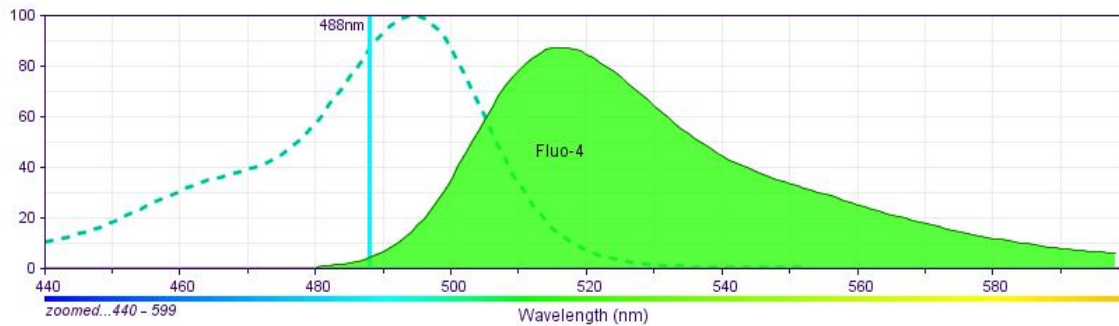
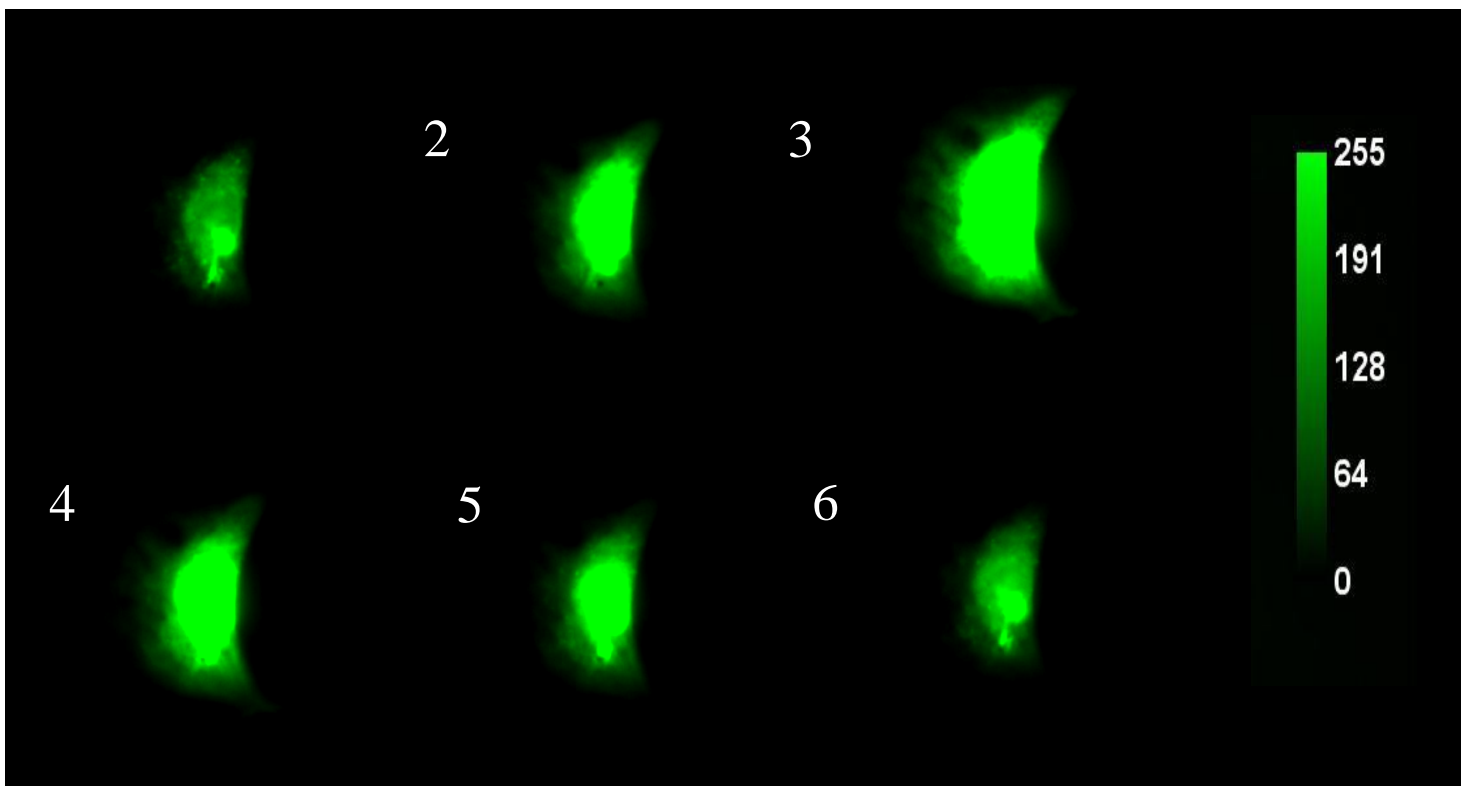


Figure. 5.4 Fluo-4 AM, excitation and emission spectra. Image showing the absorption and emission spectra of Fluo-4AM, a Calcium sensitive dye used in biology. The band at 488nm is characteristic of an Argon-ion laser. Note since 488nm is close to the absorption maximum, the emission will be close to a maximum too as discussed in chapter 2.

Appendix D. Calcium $[Ca^{2+}]_i$ Primary response sequence.

The following image shows a sub-sequence from the stack images in the movie. The scale bar to the left represents the intensity per pixel in arbitrary units. Black represents low $[Ca^{2+}]_i$ concentration and bright green represents high $[Ca^{2+}]_i$ concentration.



Appendix E. Student's TTEST.

~~The TTEST is a statistical method commonly used in biology to estimate if two or more different population distributions are statistically different.~~

The t-test is a statistical tool commonly used in biology to assess whether the means of two groups are *statistically* different from each other or not. This analysis is appropriate whenever the means of two groups, assumed to have a Gaussian distribution, are compared.

The t-test p value is given by the the ratio of the difference between the two means or averages over the noise between them.

As a note here: the TTEST assumes that the source populations reasonably follow a normal distribution, which usually requires above 40 sample components, and 10 samples ~~is~~ not comparable. More experiments are required for better statistics.

Bibliography

- [Bining, 1982] G Binnig, and H Rohrer, (1982) *Helv. Phys. Acta* 5.5, 726;
idem (1983) *Surface Sci.* 126, 236; idem (1985) *Sci. Amer.* 253,50.
- [Bining, 1986] G Binnig, C F Quate, Ch Gerber, *Atomic Force Microscope*, *Phys. Rev. Lett.* **56**, (1986).
- [Birdi, 2003]KS Birdi, *SCANNING PROBE MICROSCOPES: Applications in Science and Technology*, CRC Press (2003).
- [Drake, 1989] B Drake, CB Prater, AL Weisenhorn, SA Gould, TR Albrecht, et al. *Imaging Crystals, Polymers and Processes in Water with the Atomic Force Microscope*. *Science.* **243** (1989).
- [During, 1987] U Dürig, DW Pohl and F Rohner, *Near-field Optical-Scanning Microscopy*, *J. Appl. Phys.* **59** (1986).
- [Fukuma, 2005] T Fukuma, M Kimura, K Kobayashi, K Matsushige and H Yamada, *Development of Low Noise Cantilever Deflection Sensor for Multienvironment Frequency-Modulation Atomic Force Microscopy*, *Rev Sci Instrum* 76 053704, (2005).
- [Higgins, 2006] MJ Higgins, M Polcik, T Fukuma, JE Sader, Y Nakayama, SP Jarvis, *Structured Water Layers Adjacent to Biological Membranes*, *Biophys. J.* **91** (2006).
- [Hoh, 1991] JH Hoh, R Lal, SA John, JP Revel and MF Arnsdorf, *Atomic Force Microscopy and Dissection of Gap Junctions*. *Science* **253**, (1991).

- [Hörber1, 2003] JKH Hörber1 and MJ Miles, *Scanning Probe Evolution in Biology*, Science 302 (2003).
- [Hung, 1996] CT Hung, FD Allen, SR Pollack and CT Brighton, *Intracellular Ca^{2+} Stores and Extracellular Ca^{2+} are Required in the Real-Time Response of Bone Cells Experiencing Fluid Flow*. J. Biomech. **29** (1996).
- [LeDue, 2008] JM LeDue, M Lopez-Ayon, SA Burke, Y Miyahara and Peter Grütter, *High Q Optical Fiber Tips for NC-AFM in Liquid*, Nanotechnology 20 (2009).
- [Marti, 1987] O Marti, B Drake and PK Hansma, *Atomic Force Microscopy of Liquid-Covered Surfaces: Atomic Resolution Images*, Appl. Phys. Lett., **51**, (1987).
- [Morel, 2001] J Morel, B Combe1, J Francisco and J. Bernard, *Bone Mineral Density of 704 Amateur Sportsmen Involved in Different Physical Activities*, Osteoporos Int **12**, (2001).
- [Pervaiz, 2006] S Pervaiz, *Reactive Oxygen-Dependent Production of Novel Photochemotherapeutic Agents*. FASEB Journal, **15** (2001).
- [Pohl, 1987] DW Pohl, W Denk, and M Lanz, *Observation of Single-Particle Plasmons by Near-Field Optical Microscopy*, Appl Phys Lett, **44**,(1984).
- [Shaw, 2006] JE Shaw, J Oreopoulos, D Wong, JCY Hsu, CM Yip, *Coupling Evanescent-wave Fluorescence Imaging and Spectroscopy with Scanning TIRF-AFM*. Surf. Interface Anal. **38**, (2006).
- [Synge, 1928] EH Synge Philos. Mag. 1873, 6: 356-362.

Chapter 1

[Albercht, 1990] TR Albercht, et al., "*Frequency Modulation Detection using high Q Cantilevers for Enhanced Force Microscope Sensitivity*", J Appl Phys. 69 668 (1990).

[Attard, 2007] P Attard, *Measurement and Interpretations of Elastic and Viscoelastic Properties with the Atomic Force Microscope*, J. Phys Condensed Matter, **19**, (2007).

[Axelrod, 1990] Axelrod D., *Total internal reflection fluorescence at biological surfaces, in Noninvasive techniques in cell biology*, Wiley-Liss, New York, (1990).

[Costa, 1999] KD Costa, FCP Yin, *Analysis of Indentation: Implications for Measuring Mechanical Properties with AFM*, ASME, **121**, (1999).

[Dimitriadis, 2002] EK Dimitriadis, F Horkay, J Maresca, B Kachar, RS Chadwick, *Determination of Elastic Moduli of Thin Layers of Soft Material Using the AFM*, Biophysical J., **82**, (2002).

[Dürig, 2000] U Dürig, *Extracting Interaction Forces and Complementary Observables in Dynamic Probe Microscopy*. Appl. Phys. Lett., **76**, (2000).

[Fukuma, 2005] T Fukuma, et al., "*True atomic resolution in liquid by frequency-modulation atomic force microscopy*", Appl Phys Lett 86, (2005).

[Garcia, 2002] R Garcia and R Perez, *Dynamic AFM Methods*, Surf, Sci. Rep. **47**, (2002).

[Giessibl, 2001] FJ Giessibl, *A Direct Method to Calculate Tip-Sample Forces From Frequency Shifts in Frequency-Modulation AFM*. Appl. Phys. Lett., **78**, (2001).

- [Grandbois, 2000] M Grandbois, W Dettmann, M Benoit, HE Gaub, *Affinity Imaging of Red Blood Cells Using an AFM*, J. Histochem, Cytochem, **48**, (2000).
- [Guggisberg, 2000] M Guggisberg, M Bammerlin, Ch Loppacher, O Pfeiffer, A Abdurixit, V Barwich, R Bennewitz, A Baratoff, E Meyer and HJ Güntherodt, *Separation of Interactions by Noncontact AFM*, Phys. Rev. B, **61**, (2000).
- [Hamamatsu, 2008] *Photomultiplier Tubes Manual*, Hamamatsu, (2008).
- [Hecht, 2001] Hecht E , Zajac A , *Optics*, Addison Wesley, (2001).
- [Johnson, 1978] Johnson, *Contact Mechanics*, Cambridge University Press, Cambridge, (1978).
- [Kopycinska-Müller, 2006] M Kopycinska-Müller , RH Geiss, DC Hurley, *Contact Mechanics and Tip Shape in AFM-Based Nanomechanical Measurements*, Ultramicroscopy **106** (2006).
- [Lange, 2001] F Lange, A Cambi, R Huijbens¹, B Bakker, W Rensen, M Garcia-Parajo, N van Hulst and CG Figdor, *Cell Biology Beyond the Diffraction Limit: Near-Field Scanning Optical Microscopy*, *Journal of Cell Science* **114**, (2001)
- [Lee, 2006] M Lee and W Jhe, *General Theory of Amplitude-Modulation Atomic Force Microscopy*, Phys Rev Lett **97**, (2006).
- [Liang, 2007] XJ Liang, AQ Liu, CS Lim, TC Ayi and PH Yap, *Determining refractive index of single living cell using an integrated microchip*. Sensors and Actuators A: Physical, 133 2, (2007).
- [Martin, 1987] Y Martin and HK Wickramasinghe, *Magnetic Imaging by 'Force Microscopy' with 100 °A Resolution*, Applied Physics Letters **50**, (1987).

- [Miller, 2009] Frederic P. Miller, Agnes F. Vandome, and John McBrewhster *Microscopy: Optical Microscope, Bright Field Microscopy, Dark Field Microscopy, Dispersion Staining, Phase Contrast Microscopy, Differential Interference Contrast Microscopy, Fluorescence Microscope* (2009).
- [Olympus, 2009] *Olympus IX-71 Manual Microscope*, Olympus Corporation, (2009).
- [Otaki, 2009] T Otaki, C Howard and M Davidson, *Phase Contrast Microscopy Articles; Apodized Phase Contrast*, Nikon Corporation, (2009).
- [Paige, 2001] MF Paige, EJ Bjerneld and WE Moerner, *A Comparison of Through-the-Objective Total Internal Reflection Microscopy and Epifluorescence Microscopy for Single-Molecule Fluorescence Imaging*, *Single Mol.* 2 (2001).
- [Photometrics, 2004] *User Manual for Cascade® Systems*, Photometrics, (2004).
- [Qu, 2004] X Qu, D Wu, L Mets, and N Scherer, *Nanometer Localized Multiple Single-Molecule Fluorescence Microscopy*, *PNAS* **101**,31 (2004).
- [Radmacher, 1996] M Radmacher, M Fritz, CM Kacher, JP Cleveland and PK Hansma, *Measuring the Viscoelastic Properties of Human Platelets with the AFM* *Biophys J*, **70** (1996).
- [Schirmeisen, 2004] A Schirmeisen, H Holscher, B Anczykowski, D Weiner, MM Schafer and H Fuchs, *Dynamic Force Spectroscopy Using the Constant-Excitation and Constant-Amplitude Modes*, *Nanotech*, 16, (2004).
- [Schwarz, 1997] UD Schwarz, O Zwörner, P Köster and R Wiesendanger, *Quantitative analysis of the frictional properties of solid materials at low loads. I. Carbon compounds*, *Phys. Rev. B* 56, (1997).

- [Shulha, 2004] H Shulha, A Kovalev, N Myshkin, VV Tsukruk, *Some Aspects of AFM Nanomechanical Probing of Surface Polymer Films*, European Polymer J., **40**, (2004).
- [Smith, 2005] BA. Smith, B Tolloczko JG. Martin and Peter Grutter, *Probing the Viscoelastic Behavior of Cultured Airway Smooth Muscle Cells with Atomic Force Microscopy: Stiffening Induced by Contractile Agonist*, Biophysical Journal Volume **88**, (2005).
- [Tompkins, 2004] *MFP-3DTM Atomic Force Microscope Installation and Operation Manual*, Asylum Research Inc, (2004).
- [Tsukruk, 1998] VV Tsukruk, Z Huang, *Probing of Micromechanical Properties of Compliant Polymeric Materials*, J. of Materials Science, **33**, (1998).
- [Young, 1968] H Young, *Fundamentals of optics and modern physics McGraw-Hill Series in Fundamentals of Physics*, New York: McGraw-Hill, (1968).
- [Vanlandingham, 2005] MR Vanlandingham, NK Chang, PL Drzal, CC White, SH Chang, *Viscoelastic Characterization of Polymers Instrumented Indentation. I Quasi-Static Testing*, J. of Polymer Science, **43**, (2005).
- [Viani, 1999] MB Viani, et al., *Small Cantilevers for Force Spectroscopy of Single Molecules*. J Appl Phys **86** (1999).
- [Weisenhorn, 1992] AL Weisenhorn, P Maivald, HJ Butt, PK Hansma, *Measuring Adhesion, Attraction, and Repulsion Between Surfaces in Liquids with and AFM*, Phys Rev B, **45**, (1992).
- [White, 2005] CC White, MR Vanlandingham, PL Drzal, NK Chang, SH Chang, *Viscoelastic Characterization of Polymers Using Instrumented Indentation II*, J. of Polymer Science, **43**, (2005).
- [Yamada, 2000] S Yamada, D Wirtz and SC Kuo, *Mechanics of Living Cells Measured by Laser Tracking Microrheology*, Biophysical Journal **78** (2000).

Chapter 2

Chapter 3

- [Collin, 1995] P Collin, GA Nickols , P Osdoby, *Bone Cell Function, Regulation, and Communication: a Role for Nitric Oxide*, J Cell Biochem, **57**, (1995).
- [Corwin, 1991] Cowin, S. C., L. Moss-Salentijn, and M. L. Moss. *Candidates for the Mechanosensory System in Bone*. J. Biomech. Eng. **113** (1991).
- [Costa, 1999] KD Costa, FCP Yin, *Analysis of Indentation: Implications for Measuring Mechanical Properties with AFM*, ASME, **121**, (1999).
- [Dolmetsch, 1998] RE Dolmetsch, K Xu and RS Lewis. Calcium Oscillations Increase the Efficiency and *Specificity of Gene Expression*. Nature. **392** (1998).
- [Gee, 2000] KR Gee, KA Brown, W-NU Chen, J Bishop-Stewart, D Gray, I Johnson, *Chemical and Physiological Characterization of Fluo-4 Ca²⁺-indicator Dyes*, Cell Calcium **27**, (2000)
- [Graaff, 1998] Van De Graaff, M Kent, *Human Anatomy* 5th Edition. McGraw-Hill. Boston, MA. (1998).
- [Hassan, 1998] EA-Hassan, WF Heinz, MD Antonik, NPD'Costa, S Nageswaran, CA Schoenenberger, and JH Hoh, *Relative Microelastic Mapping of Living Cells by Atomic Force Microscopy*, Biophys J **74**, (1998).
- [Hategan, 2003] A Hategan, R Law, S Kahn and DE Discher, *Adhesively-Tensed Cell Membranes: Lysis Kinetics and AFM Probing*, Biophys J, **85** (2003).
- [Haydon et al., 1996] PG Haydon, R Lartius, V Parpura and SP Marchese-Ragonax, *Membrane Deformation of Living Glial Cells Using Atomic Force Microscopy*, J. Microsc. **182** (1996).

- [Helmke, 2002] BP Helmke and PF Davies, *The Cytoskeleton Under External Fluid Mechanical Forces: Hemodynamic Forces Acting on the Endothelium*, *Annals of Biomed Eng*, **30**, (2002).
- [Hui, 1990] SL Hui, C Slemenda, CC Johnston, *The Contribution of Bone Loss to Postmenopausal Osteoporosis*, *Osteoporos Int* **1** (1990).
- [Hung, 1996] CT Hung, FD Allen, SR Pollack and CT Brighton, *Intracellular Ca^{2+} Stores and Extracellular Ca^{2+} are Required in the Real-Time Ca^{2+} Response of Bone Cells Experiencing Fluid Flow*. *J. Biomech.* **29** (1996).
- [Jones, 1991] DB Jones, H Nolte, JG Scholubbers, E Turner, and D Velzel, *Biochemical Signal Transduction of Mechanical Strain in Osteoblast-like Cells*. *Biomaterials.* **12**, (1991).
- [Ko, 2000] KS Ko and CA McCulloch, *Partners in Protection: Interdependence of Cytoskeleton and Plasma Membrane in Adaptations to Applied Forces*, *J. Membr. Biol.* **174**, (2000).
- [Liedert, 2006] A Liedert, D Kaspar, R Blakytny, L Claes, A Ignatius, *Signal Transduction Pathways Involved in Mechanotransduction in Bone Cells*, *Biochem Biophys Res Commun*, **349** (2006).
- [Li, 2008] QS Li, GYH Lee, CN Ong and CT Lim, *AFM Indentation Study of Breast Cancer Cells*, *Biochem and Biophys Research Communications* **374** (2008).
- [Malek, 1996] AM Malek and S Izumo, *Mechanism of Endothelial Cell Shape Change and Cytoskeletal Remodeling in Response to Fluid Shear Stress*. *J. Cell Sci.* **109** (1996).
- [Morel, 2001] J Morel, B Combe, J Francisco and J. Bernard, *Bone Mineral Density of 704 Amateur Sportsmen Involved in Different Physical Activities*, *Osteoporos Int* **12**, (2001).
- [Radmacher, 1993] M Radmacher, RW Tillmann, and HE Gaub, *Imaging Viscoelasticity by Force Modulation with the Atomic Force Microscope*, *Biophys J* **64**, (1993).

Chapter 4

- [Banes, 1995] AJ Banes, M Tsuzaki, J Yamamoto, T Fischer, B Brigman, Brown and L Miller. *Mechanoreception at the Cellular Level: the Detection, Interpretation, and Diversity of Responses to Mechanical Signals*. Biochem. Cell Biol. **73** (1995).
- [Baecker, 2003] N Baecker, A Tomic, CMika, A Gotzmann, P Platen, R Gerzer, and M Heer, *Bone Resorption is Induced on the Second Day of Bed Rest: Results of a Controlled Crossover Trial*, J Appl Physiol **95**, (2003).
- [Bass, 1998] S Bass, G Pearce, E Bradney, E Hendrich, PD Delmas, A Harding, et al., *Exercise Before Puberty may Confer Residual Benefits in Bone Density in Adulthood: Studies in Active Prepubertal and Retired Female Gymnasts*. J. Bone Miner Res **13**, (1998).
- [Bonjour, 1994] JP Bonjour , G Theintz, F Law , D Slosman , R Rizzoli , *Peak Bone Mass*. Osteoporos Int, 4 Suppl 1:7-13, (1994).
- [Caillot, 1998] A Caillot-Augusseau, MH Lafage-Proust, C Soler, F Dubois and C Alexandre, *Bone Formation and Resorption Biological Markers in Cosmonauts During and After a 180-day Spaceflight*, (Euromir 95), Clin Chem **44**, (1998).
- [Charras et al., 2001] Charras, G. T., P. P. Lehenkari, and M. A. Horton, *Atomic Force Microscopy can be Used to Mechanically Stimulate Osteoblasts and Evaluate Cellular Strain Distributions*, Ultramicroscopy. **86** (2001).
- [Charras, 2002] GT Charras, MA Horton, *Single Cell Mechanotransduction and its Modulation Analyzed by Atomic Force Microscope Indentation*, Biophysical J, **82** (2002).

- [Radmacher, 1997] M Radmacher, *Measuring the Elastic Properties of Biological Samples with the AFM*, IEEE Eng. Med. Biol. Mag. **16** (1997).
- [Rico, 2005] F Rico, P Roca-Cusachs, N Gavara, R Farré, M Rotger and D Navajas, *Probing Mechanical Properties of Living Cells by Atomic Force Microscopy With Blunted Pyramidal Cantilever Tips*, Phys Rev E **72** (2005).
- [Rubin, 1984] CT Rubin and LE Lanyon, *Regulation of Bone Formation by Applied Dynamic Loads*. J. Bone Joint Surg. **66** (1984).
- [Sachs, 1998] F Sachs, CE Morris. *Mechanosensitive Ion Channels in Non-Specialized Cells*. Rev. Physiol Biochem. Pharmacol. **132**, (1998).
- [Sharmaa, 1995] RV Sharmaa, MW Chapleaua, G Hajduczuk, RE Wachtela, LJ Waitea, RC Bhallaa and FM Abboud, *Mechanical Stimulation Increases Intracellular Calcium Concentration in Nodose Sensory Neurons*, Neuroscience, **66** (1995).
- [Suominen, 1993] H Suominen , *Bone Mineral Density and Long Term Exercise. An Overview of Cross-Sectional Athlete Studies*. Sports Med. **16** (1993).
- [Takai, 2005] E Takai, KD Costa, A Shaheen, CT Hung and E Guo, *Osteoblast Elastic Modulus Measured by AFM is Substrate Dependent*. Annals of Biomed Eng. **33**, (2005)
- [Turner , 2000] RT Turner, *Physiology of a Microgravity Environment Invited Review:What do we Know About the Effects of Spaceflight on Bone?*, J Appl Physiol **89**, (2000).
- [Vauquelin, 2009]G Vauquelin, A Packeu, *Ligands, their Receptors and... Plasma Membranes*, Molecular and Cellular Endocrinology **311** (2009).